

**Publish subject to technical corrections** (16 May 2015) by Xiaobin Xu  
 Comments to the Author:

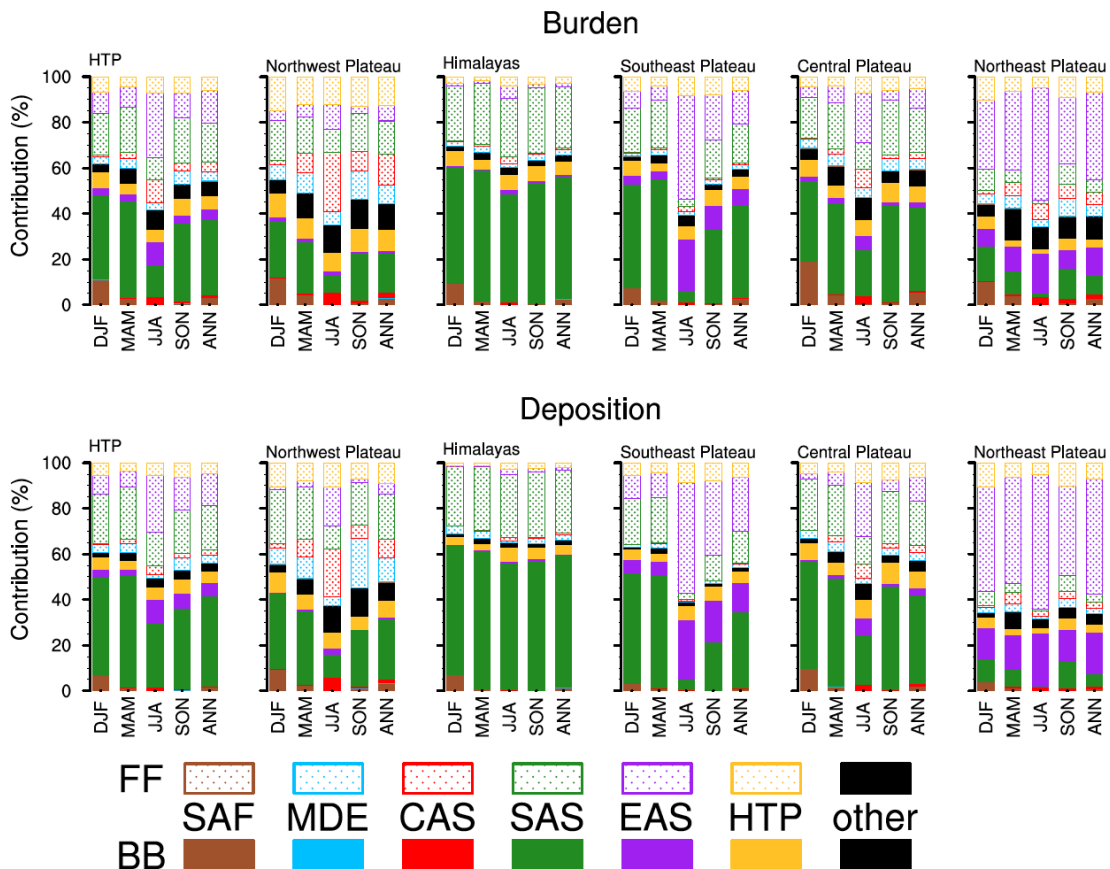
Your paper is accepted for publication in ACP. Before submitting your files for production, please make the following corrections or changes:

(1) In lines 533-534, you state "This metric has the value of 1 if the entire globe is treated as a single source region, ...", but the color scale in Fig. 7 is from 0 to 50. I guess the efficiency is x%. If so, please change the "Efficiency" in Fig. 7 to "Efficiency (%)".

Response: The values are correct. Some of the sources regions do have the efficiency greater than the global mean of 1.

(2) Fig. 6 is very difficult to understand without carefully reading the relatively long figure title. The readers will easily find there are two contributions from SAS in each case. But you have used the same color bar for BB and FF from the same region. I do not think this is a good way of displaying your results. Please use different color bars for BB and FF from the same region. If necessary you can present the deposition results in separate sub-figures.

Response: Thanks for the suggestion. We have revised the figure (see below) and make some changes to the figure caption and text accordingly.



(3) Delete "H." in line 156 and "X." in line 603.

Response: We did not use the first initials (i.e., "H." and "X.") in the original draft, but it was corrected by the copy editor during the typesetting of the discussion paper to distinguish the two references, both of which are otherwise cited as "Wang et al. (2013)".

# **Quantifying sources, transport, deposition and radiative forcing of black carbon over the Himalayas and Tibetan Plateau**

Rudong Zhang<sup>1, 2, 3</sup>, Hailong Wang<sup>2</sup>, Yun Qian<sup>2</sup>, Philip J. Rasch<sup>2</sup>, Richard C. Easter<sup>2</sup>, Po-Lun Ma<sup>2</sup>, Balwinder Singh<sup>2</sup>, Jianping Huang<sup>1</sup>, and Qiang Fu<sup>1, 3</sup>

<sup>1</sup> Key Laboratory for Semi-Arid Climate Change of the Ministry of Education, College of Atmospheric Sciences, Lanzhou University, Lanzhou 730000, Gansu, China.

<sup>2</sup> Atmospheric Sciences and Global Change Division, Pacific Northwest National Laboratory (PNNL), Richland, WA 99352, USA.

<sup>3</sup> Department of Atmospheric Sciences, Box 351640, University of Washington, Seattle, WA 98195, USA.

Manuscript for submission to *Atmospheric Chemistry and Physics*

Correspondence to: Hailong.Wang@pnnl.gov

## Abstract

1  
2 Black carbon (BC) particles over the Himalayas and Tibetan Plateau (HTP), both airborne and  
3 those deposited on snow, have been shown to affect snowmelt and glacier retreat. Since BC over  
4 the HTP may originate from a variety of geographical regions and emission sectors, it is essential  
5 to quantify the source-receptor relationships of BC in order to understand the contributions of  
6 natural and anthropogenic emissions and provide guidance for potential mitigation actions. In  
7 this study, we use the Community Atmosphere Model version 5 (CAM5) with a newly  
8 developed source tagging technique, nudged towards the MERRA meteorological reanalysis, to  
9 characterize the fate of BC particles emitted from various geographical regions and sectors.  
10 Evaluated against observations over the HTP and surrounding regions, the model simulation  
11 shows a good agreement in the seasonal variation of the near-surface airborne BC concentrations,  
12 providing confidence to use this modeling framework for characterizing BC source-receptor  
13 relationships. Our analysis shows that the relative contributions from different geographical  
14 regions and source sectors depend on season and location in the HTP. The largest contribution to  
15 annual mean BC burden and surface deposition in the entire HTP region is from biofuel and  
16 biomass (BB) emissions in South Asia, followed by fossil fuel (FF) emissions from South Asia,  
17 then FF from East Asia. The same roles hold for all the seasonal means except for the summer  
18 when East Asia FF becomes more important. For finer receptor regions of interest, South Asia  
19 BB and FF have the largest impact on BC in Himalayas and Central Tibetan Plateau, while East  
20 Asia FF and BB contribute the most to Northeast Plateau in all seasons and Southeast Plateau in  
21 the summer. Central Asia and Middle East FF emissions have relatively more important  
22 contributions to BC reaching Northwest Plateau, especially in the summer. Although local  
23 emissions only contribute about 10% of BC in the HTP, this contribution is extremely sensitive



24 to local emission changes. Lastly, we show that the annual mean radiative forcing ( $0.42 \text{ W m}^{-2}$ )  
25 due to BC in snow outweighs the BC dimming effect ( $-0.3 \text{ W m}^{-2}$ ) at the surface over the HTP.  
26 We also find strong seasonal and spatial variation with a peak value of  $5 \text{ W m}^{-2}$  in the spring  
27 over Northwest Plateau. Such a large forcing of BC in snow is sufficient to cause earlier snow  
28 melting and potentially contribute to the acceleration of glacier retreat.

29

## 30 **1 Introduction**

31 Black carbon (BC) is a distinct type of carbonaceous particulate matter mainly emitted from the  
32 incomplete combustion of fossil fuels, biofuels and biomass burning. It is the dominant insoluble  
33 light-absorbing particulate species, both in the atmosphere and after deposition on snow and ice.  
34 In addition to its impact on air quality, BC plays a unique and important role in the climate  
35 system through its effect on radiation, clouds and snow albedo, and associated feedbacks that  
36 modify atmospheric circulation patterns and/or accelerate the snowmelt and glacier retreat in the  
37 Arctic and across the mid-latitudes of the northern hemisphere (Bond et al., 2013).

38 Modeling studies (e.g., Hansen et al., 2005; Qian et al., 2011) indicate that the climate  
39 efficacy of BC in snow is much greater than efficacy of carbon dioxide or other anthropogenic  
40 forcers owing to a sequence of positive feedback mechanisms (Warren and Wiscombe, 1980,  
41 1985; Conway et al., 1996; Hansen and Nazarenko, 2004; Jacobson, 2004; Flanner et al., 2007;  
42 Ye et al., 2012; Hadley and Kirchstetter, 2012; Doherty et al., 2014). Flanner et al. (2009)  
43 demonstrated that the global annual BC snow-albedo effect (darkening) outweighs the aerosol  
44 (BC and organic matter) dimming effect (i.e., reduced the downwelling irradiance reaching the  
45 surface) by a factor of about 6. The snow/ice-covered Himalayas and Tibetan Plateau (HTP)  
46 region is more prone to these BC effects than other regions because of the surrounding two major

47 BC source regions, East Asia and South Asia, at present and likely in the future (e.g., Bond et al.,  
48 2007; Ohara et al., 2007; Xu et al., 2009; Lamarque et al., 2010; Menon et al., 2010).

49 The HTP, often referred to as the Third Pole, has received much less scientific attention  
50 than the Polar Regions (Qiu, 2008), although it is the highest and largest plateau that stores one  
51 of the largest ice masses of the Earth system. The HTP also has a large area of seasonal and  
52 permanent snow cover and represents the most sensitive and visible indicator of climate change  
53 with its unique location for complex interactions among the atmosphere, hydrosphere and  
54 cryosphere (e.g., Pu et al., 2007; Xu et al., 2009; Yao et al., 2012). The glaciers and the  
55 associated snowmelt over the HTP have a great potential to modify the regional hydrology and to  
56 trigger natural hazards that impact a large portion of the population in and around the region (e.g.,  
57 Barnett et al., 2005; Singh and Bengtsson, 2004; Xu et al., 2008; Kaser et al., 2010; Immerzeel  
58 et al., 2010; Yao et al., 2012; Bolch et al., 2012). The HTP also exerts profound influences on  
59 atmospheric circulation patterns and climate through mechanical and thermal effects due to its  
60 large area, highly elevated topography and geographical location in the Earth system (Yeh et al.,  
61 1957; Manabe and Terpstra, 1974; Ye and Gao, 1979; Yanai et al., 1992; Ye and Wu, 1998; Wu  
62 et al., 2012). The HTP acts as a giant wall across the Eurasian continent that blocks cold  
63 outbreaks from high latitudes in winter and confines the winter monsoon to eastern and southern  
64 Asia, while in summer the HTP serves as a huge heat source through the strong surface sensible  
65 heating and latent heating over central and eastern Plateau (Wu et al., 2012).

66 Under the background of global warming, the climate of the HTP is changing rapidly. For  
67 example, the surface sensible heat flux has weakened in recent decades, mainly due to global  
68 warming (Duan and Wu, 2008). Observational evidence indicated that the surface air  
69 temperatures on the HTP have increased about 1.8°C over the past 50 years (Wang et al., 2008),

70 while the large area at elevations above 4000 m has warmed at 0.3°C per decade in the past three  
71 decades (Xu et al., 2009). A number of recent studies reported that glaciers on the HTP have  
72 undergone widespread losses at an increasing rate in past decades (e.g., Qin et al., 2006; Li et al.,  
73 2008; Kang et al., 2010; Bolch et al., 2012) and have undergone accelerated retreat in recent  
74 years (Yao et al., 2007). The rapid warming and the accelerated glacier retreat have been  
75 primarily attributed to increasing greenhouse gases (e.g., Duan et al., 2006; Ren et al., 2006), but  
76 other factors may be partly responsible for the accelerated warming over the HTP, such as  
77 atmospheric heating by absorbing aerosols, land use changes, and reduction of snow albedo  
78 induced by light-absorbing impurities in snow (Kang et al., 2000; Prasad and Singh 2007;  
79 Ramanathan et al., 2007; Flanner et al., 2007, 2009; Yasunari et al., 2010; Xu et al., 2009; Qian  
80 et al., 2011, 2015). Lau et al. (2006, 2010) proposed and demonstrated the Elevated Heat Pump  
81 mechanism, whereby heating induced by airborne BC and dust absorption can strengthen local  
82 circulations and lead to a northward shift of the monsoon rain belt, widespread enhanced  
83 warming over the HTP, and accelerated snowmelt and glacier retreat. Previous observational and  
84 modeling studies have indicated that BC deposition on snow and ice, which has a rapidly  
85 increasing trend in recent years, has been a significant contributor to the early snowmelt and  
86 rapid glacier retreat over the HTP (e.g., Flanner et al., 2007, 2009; Ming et al., 2008; Xu et al.,  
87 2009; Kaspari et al., 2011; Menon, et al., 2010; Qian et al., 2011, 2015; Wang et al., 2015).  
88 Flanner et al. (2007) found that the largest regional annual mean forcing due to BC in snow is  
89 located in the HTP. Xu et al. (2009) and Lau et al. (2010) suggested that the BC in snow/ice may  
90 be partly responsible for the observed acceleration of glacier retreat in the HTP.

91         Understanding the role of BC in accelerating snow-cover reduction and glacier retreat is  
92 becoming increasingly important. Over 60% of BC in the present-day atmosphere originates

93 from anthropogenic activities (e.g., Bond et al., 2007; Lamarque et al., 2010). Reduction of  
94 emissions from BC-rich sources represents a potential mitigation strategy to slow down present-  
95 day climate change because BC has a positive radiative forcing but a short atmospheric lifetime  
96 (Bond et al., 2013). Since BC over the HTP may originate from a variety of geographical regions  
97 and emission sectors, it is essential to quantify the source-receptor relationships of BC in order to  
98 understand the contributions of open fire and anthropogenic emission sectors to BC over the  
99 HTP. This exercise is also essential to provide guidance for potential mitigation actions.

100         Some studies have used the conventional back-trajectory approach to identify possible  
101 source regions for both airborne BC and that deposited on snow and ice, by tracking air mass  
102 reaching sampling sites over the HTP (e.g., Ming et al., 2008, 2009; Cao et al., 2009; Bonasoni  
103 et al., 2010; Zhao et al., 2013; Zhang et al., 2013). Lu et al. (2012) developed a novel back-  
104 trajectory approach to analyze the origin of BC transported to the HTP during 1996-2010. They  
105 derived the overall transport characteristics of BC to the HTP and showed the spatial distribution  
106 of sources for BC reaching the HTP region based on a large set of seven-day back trajectories  
107 arriving at the given height (i.e., 500 m) and receptor locations, BC emissions and transport  
108 efficiencies. The statistical analysis of trajectories has good accuracy on short time scales for  
109 source regions with close proximity to the receptor, but this approach has limitations in  
110 determining contributions from distant sources to BC in the mid- and upper-troposphere that  
111 could contribute significantly to the total column burden but less to BC deposition and boundary-  
112 layer concentrations. Using the adjoint of the GEOS-Chem global chemical transport model,  
113 Kopacz et al. (2011) attempted to identify the originating locations of BC arriving at five glacier  
114 sites (i.e., five model grid-cells as the receptors) in the HTP for year 2001. This method can  
115 provide a global distribution of emissions that directly contribute to BC concentrations at

116 receptor locations. Note that the adjoint model results are not source attributions but rather the  
117 source-receptor sensitivities, which can be interpreted as the effectiveness of incremental  
118 changes to existing emissions in affecting BC at receptor locations. While the adjoint approach  
119 has the advantage of not predefining source regions, it does require performing separate  
120 simulations for each of the defined receptor regions.

121 In this study, we use an aerosol-climate model with a newly developed explicit source  
122 tagging approach (Wang et al., 2014) to produce a detailed characterization of the fate of BC  
123 emitted from various geographical regions and sectors (e.g., fossil fuel, biofuel and biomass  
124 burning emissions) and transport pathways to the HTP. In contrast to the back-trajectory and the  
125 adjoint approaches, the direct tagging method has the flexibility to do source attribution of BC  
126 mass mixing ratio at any model layer and the surface dry and/or wet deposition within a single  
127 simulation for any receptor regions. Section 2 describes the aerosol-climate model and the  
128 tagging method used in this study. Section 3 presents an evaluation of modeled BC surface  
129 concentrations and seasonal snow cover over the HTP region. The transport pathways and source  
130 attribution results are presented in Sect. 4. The radiative effects of BC in the atmosphere and of  
131 both BC and mineral dust in snow are compared in Sect. 5, followed by the summary and  
132 conclusions in Sect. 6.

133

## 134 **2 Model Configuration and Experimental Design**

### 135 **2.1 The CAM5 model and the source-tagging method**

136 We use the Community Atmosphere Model Version 5 (CAM5; Neale et al., 2012), which is the  
137 atmospheric component of the Community Earth System Model version 1 (CESM1) (Hurrell et  
138 al., 2013). It includes relatively comprehensive representations of aerosols and clouds, and

139 mechanisms for their interactions with each other and with climate (Gettelman et al., 2010; Liu  
140 et al., 2012). CAM5 employs a modal aerosol module (MAM) to represent aerosols in multiple  
141 log-normally distributed modes, with internal mixing assumed for aerosol species within each  
142 individual mode, including a 3-mode standard representation (MAM3) and a more complex 7-  
143 mode representation (MAM7). The major difference between MAM3 and MAM7 related to  
144 carbonaceous aerosols lies in the treatment of aging. In MAM3, BC and primary organic matter  
145 (POM) particles are emitted into the accumulation mode that also contains highly hygroscopic  
146 species such as sulfate and sea-salt, while in MAM7 BC and POM are emitted into a primary  
147 carbon mode, which contains no other species. BC is hydrophobic upon emission, and thus the  
148 hygroscopicity of the primary-carbon-mode particles depends on the assumed hygroscopicity for  
149 POM. As more hygroscopic species (e.g.,  $\text{H}_2\text{SO}_4$  and  $\text{NH}_3$ ) condense onto the primary-carbon-  
150 mode particles, the particles are become more hygroscopic and are gradually transferred into the  
151 MAM7 accumulation mode. The rate of transfer is controlled by uncertain aging parameters, and  
152 the availability of gas precursors (Liu et al. 2012). In the accumulation mode of both MAM3 and  
153 MAM7, BC is internally mixed with other more hygroscopic species and is thus subject to wet  
154 scavenging and removal processes. During the transport from sources to remote regions, aerosols  
155 are removed too efficiently in the default CAM5 (Liu et al., 2012). Recently, H. Wang et al.  
156 (2013) revised some key processes associated with aerosol wet removal and convective transport,  
157 which significantly improved the vertical distribution of aerosols and their transport to remote  
158 regions such as the Arctic.

159 To better characterize the sensitivity of BC spatial distributions to emission uncertainties,  
160 Wang et al. (2014) implemented a direct source tagging method in CAM5, whereby BC emitted  
161 from a number of independent source regions and/or sectors can be tagged and explicitly tracked

162 within a single model simulation. This approach provides the quantitative characterization of  
163 source-receptor relationships for BC in any receptor region without perturbing emissions from  
164 individual BC source regions or sectors. In this study, we apply the BC tagging technique to the  
165 accumulation-mode BC in the MAM3 treatment. BC particles emitted from sixteen geographical  
166 BC source regions and two emissions sectors (i.e., biomass burning & biofuel emissions and  
167 fossil fuel emissions) in each of the regions are tagged and explicitly tracked. Instead of using  
168 the global emissions from all sectors for the original one BC mass mixing ratio variable, the  
169 thirty two regional/sectoral emissions provide sources to the respective tagged BC mass mixing  
170 ratio variables that are all added to the accumulation mode, including both interstitial and cloud-  
171 borne states. All physical and dynamic tendencies (e.g., transport, dry and wet removal) are  
172 calculated explicitly for the tagged BC mass mixing ratio variables in the same way as the  
173 original single BC mass mixing ratio. Also, when aerosol optical properties are calculated, all of  
174 the tagged BC mass mixing ratios contribute to the volume-mean refractive index of the  
175 accumulation mode that is used in the radiation calculation.

176 In addition to the free-running mode, CAM5 can also be configured in an offline mode,  
177 in which temperature, wind, surface fluxes (heat, moisture, and momentum), and pressure are  
178 constrained to agree closely with observations, while clouds and aerosol are allowed to evolve  
179 freely (Rasch et al., 1997; Lamarque et al., 2012; Ma et al., 2013). In this study, we run the  
180 CAM5 model in the offline mode with the direct BC source tagging capability, including the  
181 improved representation of convective transport and wet removal of aerosols. We use the NASA  
182 Modern Era Retrospective-Analysis for Research and Applications (MERRA) reanalysis dataset  
183 (Rienecker et al., 2011), using a horizontal resolution of  $1.9^\circ \times 2.5^\circ$  and 56 vertical levels. The  
184 goal is to characterize the fate of BC emitted from various geographical regions and sectors, their

185 transport pathways to the HTP, and their radiative forcing with seasonal variations. The  
186 simulation is performed for year 2001 with prescribed sea surface temperatures.

## 187 **2.2 BC source regions and sectors**

188 BC emission datasets have large uncertainties (e.g., Bond et al., 2013), and there are different  
189 inventories available for climate modeling. We use the present-day (i.e., year 2000) monthly  
190 mean emission inventories for BC provided by Lamarque et al. (2010). They were built for the  
191 climate model simulations in the Coupled Model Intercomparison Project Phase 5 (CMIP5)  
192 (Taylor et al., 2012) performed for the fifth assessment report (AR5) of the Intergovernmental  
193 Panel on Climate Change (IPCC). The AR5 BC emissions being used in our CAM5 simulation  
194 include monthly varying elevated open fire emissions (injection altitude up to 6 km), and yearly  
195 constant surface emissions from shipping and from six sectors over land: agricultural waste  
196 burning, domestic, energy, industry, transportation, and waste treatment. These surface BC  
197 emissions sectors do not distinguished between biofuel and fossil fuel combustion. To prepare  
198 for the BC source sector tagging, we divide the total surface emissions into two broader sectors,  
199 biofuel and fossil fuel, by using the ratio of biofuel to biofuel plus fossil fuel at each model grid  
200 provided by Dentener et al. (2006). We then combine the biomass burning (open fire) emissions  
201 and surface biofuel emissions, hereafter, referred to as BB (biofuel and biomass) sector. The  
202 shipping emissions are combined with the fossil fuel emissions over land to form the FF (fossil  
203 fuel) sector. Note that emissions in the BB sector have seasonal variations (associated with the  
204 open fire emissions) but the FF sector emissions used in this study have no seasonal variation at  
205 all.

206 The sixteen geographical BC source regions (Fig. 1a) are defined using the definition of  
207 source/receptor regions by Work Plan (WP 2.1) of the Task Force on Hemispheric Transport of



208 Air Pollution (<http://iek8wikis.iek.fz-juelich.de/HTAPWiki/WP2.1>). They are ARC (Arctic),  
209 NAM (North America), CAM (Central America), SAM (South America), EUR (Europe), NAF  
210 (North Africa), SAF (South Africa), MDE (Middle East), CAS (Central Asia), SAS (South Asia),  
211 EAS (East Asia), SEA (South East Asia), PAN (Pacific, Australia and New Zealand), RBU  
212 (Russia, Belarus and Ukraine), HTP (Himalayas and Tibetan Plateau) and ROW (Rest of World).

213 Figure 1b and Table S1 in the Supplement summarize the fractional contributions of BC  
214 emissions from the different source regions and sectors. The global annual mean BC emission  
215 rate is  $7.78 \text{ Tg yr}^{-1}$ , with 56.2% (sum of the red bars) from BB emissions (33.6% from fires and  
216 22.6% from biofuel) and 43.8% (sum of the blue bars) from FF emissions. The two largest  
217 contributors are BB emissions from SAF (about 20%) and FF emissions from EAS (about 15%),  
218 followed by BB emissions from SEA (7.7%), EAS (6.4%), SAS (6.2%) and SAM (5.7%), and  
219 EUR FF (6.4%) emissions. The geographical distributions of BC annual mean emission fluxes  
220 from BB and FF sectors for year 2000 are shown in Fig. S1 (in Supplement). The global annual  
221 and seasonal mean lifetime of BC emitted from the tagged source regions and sectors are  
222 summarized in Table S2. On the globe average, BB BC has a longer lifetime than FF BC in all  
223 seasons, especially in boreal winter (6.9 vs. 3.1 day), due in part to higher open-fire emissions (in  
224 the BB sector) during local dry seasons. Another reason is that open-fire emissions have initial  
225 injection heights of up to 6 km, resulting in less removal below 6 km. The availability of co-  
226 emitted hygroscopic species that are internally mixed with BC in the accumulation mode of the  
227 MAM3 aerosol treatment also impacts the scavenging and wet removal rate of BC. This also in  
228 part explains the variability of BC lifetime among the different source regions and sectors.  
229 Regarding the seasonal cycle, BC emitted from the major source regions (e.g., SAF, EAS, SEA,

230 SAS) has substantially lower lifetime in summer (JJA) than in the other seasons, likely due to  
 231 relatively strong removal by the summer monsoon precipitation.

232 We use two metrics for quantifying source-receptor relationships and the sensitivity of  
 233 BC in a receptor region to various sources following Wang et al. (2014), but we extend them to  
 234 treat BB and FF sectors separately.

235 1) The fractional contribution of BB and FF emissions from source region  $i$  to a BC property in  
 236 receptor region  $j$  (the entire HTP or a subset of it),  $C_i^{BB}$  or  $C_i^{FF}$ , is defined as

$$237 \quad C_i^{BB} = \frac{A_i^{BB}}{A_j}, C_i^{FF} = \frac{A_i^{FF}}{A_j} \quad (1)$$

238 Where  $A_i^{BB}$  and  $A_i^{FF}$  are a BC property (e.g., mass mixing ratio, column burden, or deposition  
 239 flux) in/over receptor region  $j$  resulting from BB and FF emissions, respectively, in source region  
 240  $i$ , and  $A_j = \sum_{i=1}^N (A_i^{BB} + A_i^{FF})$  represents the total BC property in the receptor region from all  
 241 source regions ( $N = 16$  in this study) and sectors (BB and FF). Note that for BC properties such  
 242 as column burden, surface mixing ratio, and deposition flux, the tagging method in CAM5  
 243 explicitly calculates how much is due to emissions from each source region and sector.

244 2) The efficiency of BB and FF emissions from source region  $i$  in changing BC in a receptor  
 245 region  $j$  is defined as

$$246 \quad S_i^{BB} = \frac{C_i^{BB}}{E_i^{BB}/E_{tot}}, S_i^{FF} = \frac{C_i^{FF}}{E_i^{FF}/E_{tot}} \quad (2)$$

247 Where  $C_i^{BB}$  and  $C_i^{FF}$  are the fractional contribution defined in Eq. (1), and  $E_i^{BB}$  and  $E_i^{FF}$  are the  
 248 total BB and FF emission rates, respectively, in source region  $i$ , and  $E_{tot} = \sum_{i=1}^N (E_i^{BB} + E_i^{FF})$  in  
 249 Eq. (2) represents the global total emission rate. The efficiency metric  $S_i^{BB}$  or  $S_i^{FF}$  characterizes  
 250 the sensitivity of aerosol properties in a receptor region to per unit (BB or FF) emissions in  
 251 source region  $i$ . As noted in Wang et al. (2014), the efficiency is proportional to the metric of

252 relative contribution per unit source region emission used by Shindell et al. (2008). Physically,  
253 the efficiency metric can be viewed as the efficiency of transport from a source region to the  
254 receptor region. This metric is perhaps of more interest to policy makers for the purpose of  
255 mitigation action, which is not the focus of this study but is worth mentioning.

256

### 257 **3 Model evaluation against available observations**

258 The CAM5 model has been evaluated in detail from different perspectives with available  
259 observations such as aerosol mass concentration, aerosol number concentration and size  
260 distribution, aerosol optical properties, cloud properties, aerosol deposition and BC in snow over  
261 various regions in previous studies (Liu et al., 2012; H. Wang et al., 2013; Ma et al., 2013; Jiao  
262 et al., 2014; Lee et al., 2013; Qian et al., 2014). Because of the complex topography and  
263 meteorology of the HTP and the relatively coarse resolution of global model, further model  
264 evaluation focusing on the HTP region is critical. Here we use near-surface atmospheric BC  
265 concentrations measured at a few HTP sites and the snow cover fraction retrieved from satellite  
266 to evaluate the CAM5 performance in the HTP.

#### 267 **3.1 Atmospheric BC surface concentration**

268 There are seven remote sites that have surface measurements of seasonal BC aerosol  
269 concentrations available. The locations and elevations of the sites and the sampling time periods  
270 and observation methods are described in Table 1. Figure 2 shows the comparison of seasonal  
271 mean BC concentrations between observations and CAM5 results. Note that model results  
272 represent mean concentrations in the grid box that the sampling sites reside in and at the grid-  
273 mean elevation, which could deviate significantly from the sampling point near complex terrain.  
274 All sites have non-negligible amounts of BC in the near-surface air. The error bars indicate the

275 intra-seasonal and inter-annual variations if multi-year data were used for given season and site.  
276 However, the uncertainties of observed BC surface concentrations mainly originate from the  
277 large discrepancies between different measurement methods, the mixing of BC with other  
278 components (e.g., organic carbon and mineral dust) in the aerosol samples, and the sampling  
279 time and location (Bond et al., 2013; Petzold et al., 2013). BC surface concentrations over the  
280 various sites show strong seasonal variations, which are reasonably captured by the model. The  
281 modeled magnitude of BC concentrations has a good agreement with observations at some sites  
282 (e.g., Fig. 2b, d, g), but the model clearly overestimates BC at the Muztagh Ata site (Fig. 2a) and  
283 underestimates at the Lulang site (Fig. 2e). The large underestimation (about 1000 m; see Table  
284 1) of the Muztagh Ata site elevation in the model, determined by the model grid resolution, could  
285 largely explain the overestimation of BC since BC concentrations have sharp decreases with  
286 height in this region. At the sites over southern HTP (i.e., Hanle, Manora Peak, NCO-P, Lulang  
287 and NCOS), the BC surface concentrations in the summer (JJA) are lower, mainly due to wet  
288 scavenging by more frequent precipitation and partly due to the minimal emissions from  
289 domestic heating and wildfires over Himalaya foothills and Indo-Gangetic Plains (IGP) during  
290 the Indian summer monsoon season (Marinoni et al., 2010, 2013). Among all these sites, the  
291 largest BC surface concentrations occur at the Manora Peak site that is closer to the major  
292 sources in South Asia, especially in the winter (DJF) when the model underestimates the  
293 concentrations by about 50%. The high concentrations in winter at Manora Peak is mainly due to  
294 the dry winter monsoon conditions and increased transport of emissions from regional biomass  
295 burning, agricultural waste and wood fuel burning from the IGP (e.g., Ram et al., 2010; Moorthy  
296 et al., 2013). The BC surface concentrations peak in the springtime (MAM) at Hanle, NCO-P,  
297 Lulang and NCOS sites. This might be related to an increase in BB and/or FF emissions in the

298 Indian Subcontinent, along with the higher regional boundary-layer top over the IGP during the  
299 springtime that may favor the transport of particles from the surface up to higher altitudes (e.g.,  
300 Marinoni et al., 2010, 2013). Moreover, a long-range transport of pollution emitted from distant  
301 regions like the Middle East, North Africa or Europe (Marinoni et al., 2010) could further  
302 contribute to BC variability over the South Himalayas, which will also be examined in this study.  
303 Part of the discrepancies between observations and model results can be attributed to the inherent  
304 difficulty in simulating the cloud/precipitation fields over the complex topography and  
305 subsequent wet removal of aerosols during the transport, but emission uncertainties (e.g., Bond  
306 et al., 2013) might play a primary role.

### 307 **3.2 Snow cover fraction**

308 It is important to evaluate the performance of model in simulating seasonal snow over this region  
309 in order to assess the importance of BC-in-snow effect. Figure 3 shows the CAM5 simulated  
310 seasonal and annual mean snow cover fraction (SCF) during year 2001, in comparison to  
311 observed mean SCF, derived from the Moderate Resolution Imaging Spectrometer (MODIS)  
312 (Hall et al., 2006) monthly mean of daily products at 0.05 degree resolution. For a better  
313 comparison, the MODIS monthly mean SCFs are mapped to the CAM5 grid. The summer (JJA)  
314 season only includes July and August for both CAM5 and MODIS due to missing MODIS data  
315 in June 2001. To illustrate whether year 2001 can represent the average condition in terms of  
316 SCF, the MODIS SCF climatology (2000-2013) is also plotted. The overall SCF in HTP has very  
317 small difference between climatology and year 2001 in all seasons except for JJA, when SCF is  
318 notably higher over northwest Plateau for the climatology that included June SCF in the average.  
319 On average, SCF is about 5% (absolute amount) higher in June than in July and August. Over the  
320 52 HTP grid cells, the CAM5 SCF is highly correlated spatially with that of MODIS (for both

321 2001 and 2000-2013) with the statistical confidence level greater than 99%, except for summer  
322 (JJA) when the linear correlation is significant only at 80% level.

323         There are strong spatial and seasonal variations in SCF due to the complex terrain and  
324 seasonal variation in snowfall and melting. The SCF over the entire HTP reaches the maximum  
325 in the winter (DJF), while decreases to almost none (less than 5%) in July and August. Snow  
326 covers the western and southeastern Plateau during the transition seasons (MAM and SON). The  
327 CAM5 simulation shows a good agreement with MODIS in the annual mean (ANN) SCF and the  
328 strong seasonality. The most persistent snow cover at the southern and western edges of the HTP  
329 and the relatively less persistent in the HTP interior are captured by the CAM5 model. The  
330 performance of the CAM5 has been improved, in comparison to its earlier version (CAM3) that  
331 remarkably overestimated the SCF especially over the HTP interior (Qian et al., 2011), although  
332 the CAM5 still significantly overestimates the SCF in the western Plateau in DJF and MAM and  
333 underestimates it in JJA. The CAM3 model used by Qian et al. (2011) overestimates SCF by up  
334 to a factor of 2 during the cold season (November to April). The CAM3 spring (MAM) mean  
335 SCF is greater than 35%, while the CAM5 spring mean (21%) in the present study is in good  
336 agreement with the MODIS spring SCF ( $18\pm 5\%$ ).

337         Although we believe that the CAM5 SCF biases are qualitatively robust, it is worth  
338 noting that the MODIS products have uncertainties as well. Pu et al. (2007) evaluated the  
339 MODIS SCF products over the HTP against ground-based snow observations and showed that  
340 total error in MODIS SCF products over the HTP is about 10%. However, their analysis based  
341 on MODIS eight-day snow-cover composite gave a significantly higher SCF (more than 10%)  
342 than the one we show here using daily products, especially, in winter and early spring.  
343 Interestingly, based on a different source of observation, Qin et al. (2006) found that snow covers

344 about 59% of the Tibetan Plateau in winter, which is comparable to the mean SCF (50%) in our  
345 CAM5 simulation. Nonetheless, we keep this discrepancy in mind when interpreting the  
346 wintertime BC-in-snow radiative forcing that suffers the most from such potential SCF bias.

347

## 348 **4 Modeled transport pathways and source attribution of BC in the HTP**

### 349 **4.1 Transport pathways**

350 The direct source tagging method can clearly characterize the three-dimensional transport  
351 pathways of BC emitted from various source regions and sectors to the HTP receptor region.  
352 General circulation patterns over the HTP and surroundings are typically affected by mid-latitude  
353 westerlies in the winter and Asian monsoon in the summer, including the South Asian summer  
354 monsoon and East Asian summer monsoon (Xu et al., 2009; Yao et al., 2012; Wu et al., 2012;  
355 also see Fig. S2).

356 Figure 4 illustrates circulation patterns over HTP and BC transport pathways from six  
357 major source regions to the HTP in the winter (DJF) and summer (JJA). (See similar plots in  
358 Figs. S3–S5 for other tagged source regions.) In the winter, the strong surface cooling over the  
359 HTP leads to subsidence/divergence and the formation of an enhanced local circulation cell,  
360 while in the summer air converges toward the HTP from the surroundings, particularly from the  
361 South Asia, due to the ascending of strongly heated air over the HTP (e.g., Wu et al., 2012), as  
362 also indicated by the arrows in the vertical cross-sections in Fig. 4. In the winter, the subtropical  
363 westerlies extend to about 10°N in mid-/upper troposphere and 20°N near surface, and the  
364 tropical easterlies are weak (see the white contours of latitude-height cross-section panels in Fig.  
365 4). The circulation patterns near the HTP change dramatically during the summer monsoon

366 season. The reversal of surface wind regime in the tropics (e.g., Arabian Sea, Bay of Bengal, and  
367 South China Sea) is characteristic of the Asian summer monsoon climate (see Fig. S2e, g). The  
368 subtropical westerlies recede to north of 30°N and the center of the westerly jet shifts to about  
369 40°N in JJA (from about 30°N in DJF). The strong easterlies characterize the upper troposphere  
370 of tropical region (south of HTP), while the southwesterly flow prevails in the lower troposphere  
371 (white contours of latitude-height cross-section panels in Fig. 4). The prevailing winds during the  
372 transition seasons (MAM and SON) between DJF and JJA are still westerlies (Fig. S2b, d).

373         The circulation patterns determine the transport of BC around the HTP region. However,  
374 the variations of spatial distributions of BC emitted from the different source regions and in  
375 different seasons could be due to the differences in source location and strength, wet removal  
376 rate and lifting. Note that although we combined BC emitted from BB and FF sections to  
377 characterize transport pathways in Fig. 4, only BC emissions from BB sector have seasonal  
378 variations in the emission inventory we use.

379         The HTP region is surrounded by two major BC source regions, SAS and EAS (Fig. 1a),  
380 which potentially have great impact on BC in the HTP (e.g., Menon et al., 2010; Bond et al.,  
381 2007; Ohara et al., 2007; Xu et al., 2009; Kopacz et al., 2011; Lu et al., 2012). BC emissions  
382 from SAS are dominated by the BB sector, and by FF sector from EAS (Fig. 1b). As shown in  
383 Fig. 4, in the winter, a significant amount of BC from SAS can be transported to the eastern  
384 Plateau by the strong westerlies under the dry winter monsoon conditions. During the South  
385 Asian summer monsoon BC from SAS is effectively removed by the local abundant  
386 precipitation, as indicated by the low lifetime in summer (Table S2), but can still affect large area  
387 in the southwest of the HTP. However, BC from EAS can be uplifted higher and transported  
388 more to the Northeast Plateau in the summer monsoon season than in the winter. Along the



389 wintertime westerlies, BC from upwind source regions (e.g., EUR, NAF, SAF, MDE, and CAS;  
390 see Fig. S3) can easily move to the HTP, while the HTP local emissions are transported far away  
391 (Fig. 4). BC originating from the distant sources such as SAF and MDE reaches up high (to  
392 300hPa) in the HTP. In the summer, continental deep convection can loft BC into higher  
393 altitudes where it can be transported to the HTP along the relatively weaker westerlies from  
394 upwind source regions (e.g., EUR, RBU, MDE, and CAS; see Figs. 4 and S3). However, BC  
395 from distant low-latitude source regions such as SAF barely reaches the HTP region due to weak  
396 emissions but strong removal along the transport pathways to the HTP during the summer  
397 monsoon season.

#### 398 **4.2 Seasonal variation of BC in the HTP**

399 BC concentrations in the HTP have strong dependence on season and location. Figure 5 shows  
400 the annual mean and seasonal variations of BC column burden and deposition rate over the HTP  
401 and five sub-regions. The seasonal variation of the ratio of wet to total BC deposition is  
402 superimposed. The Central Plateau is the cleanest region during all seasons, compared to other  
403 sub-regions in the HTP (Fig. 5e). Both BC column burden and deposition rate from the BB  
404 sector peak in MAM over the HTP, mostly in the Himalayas and Southeast Plateau region. The  
405 FF BC burden in the HTP peaks in the summer mainly due to the seasonal maximum over  
406 Northwest and Northeast Plateaus. However, BC wet removal rate over the Northwest Plateau is  
407 at minimum in the summer, as opposed to the summer maximum in other sub-regions and the  
408 entire HTP region. For Himalayas, Southeast and Central Plateau, the seasonal variation (i.e.,  
409 maximum in MAM followed by a sharp decrease to JJA) of BB and FF column burden (Fig. 5c,  
410 d and e) is similar to the variation of observed surface concentrations at sites located in these  
411 sub-regions (Fig. 2b, d, e and f). In the Himalayas and Southeast Plateau, the ratio of regional

412 mean BC column burden to deposition rate (Fig. 5c and d), indicator of removal time scale or  
413 lifetime, is the smallest (less than 1 day) during the Asian summer monsoon (JJA) due to the  
414 efficient wet scavenging of BC by abundant precipitation. In Northwest and Northeast Plateau,  
415 the BC column burden increases from DJF to JJA and reaches the maximum in JJA, and then  
416 decreases in SON (Fig. 5b and f), partly due to the peak contribution of EAS and CAS emissions  
417 in JJA. This trend is also similar to that in the observed surface concentrations (Fig. 2a and g).  
418 The deposition rate follows the same seasonal variation of column burden over the Northeast  
419 Plateau, while the deposition has a minimum in JJA over the Northwest Plateau when the column  
420 burden is at maximum likely due to the less efficient wet removal in this region (Fig. 5b and f).

421 The annual mean BC column burden over the HTP has almost the same contributions  
422 from BB and FF emission origins, with BB dominating in DJF and MAM and FF in JJA. In the  
423 Himalayas, BC is predominantly from BB sector for all seasons (Fig. 5c). In the Southeast and  
424 Central Plateaus, the dominant source sector is BB in DJF and MAM, but FF dominates in JJA.  
425 The dominant source sector over the Northwest and Northeast Plateaus is always FF, especially  
426 in the summer. We need to analyze the source-receptor relationships in order to quantify the  
427 roles of BB and FF emissions from the various source regions in determining BC over the HTP  
428 and the sub-regions.

#### 429 **4.3 BC source-receptor relationships**

430 Previous studies (e.g., Xu et al., 2009; Kopacz et al., 2011) have shown that BC and its source-  
431 receptor relationships vary significantly with season and location in the HTP. We intend to  
432 quantify source contributions to BC at different locations of the HTP and in different seasons.  
433 Our analysis also shows that the relative contributions to BC from different source regions and

434 sectors depend on season and location in the HTP. As shown in Fig. 6, the largest contribution to  
435 the annual mean BC burden and surface deposition for the entire HTP region is from BB  
436 emissions from SAS, followed by FF emissions from SAS and then the FF from EAS. The same  
437 roles hold for all the seasonal means except for the summer (JJA) when the EAS FF becomes  
438 more important for BC column burden in the HTP and, to a lesser extent, for deposition.

439 The SAS emissions account for 50% of the annual mean burden over the HTP, including  
440 33% from BB and 17% from FF. The other 50% is mostly from the EAS (5% BB and 14% FF),  
441 HTP (6% BB and 6% FF), CAS FF (4%), MDE FF (4%) and SAF BB (3%). The source  
442 attribution for annual mean BC deposition for the entire HTP is similar, but SAS contributes  
443 even more to BC deposition than to the column burden. Although RBU has a lower contribution  
444 to the annual mean BC in the HTP than the six regions shown in Fig. 6, its contribution to the  
445 JJA mean, especially at some locations, is quite substantial (included in the black bar) and even  
446 more important than some of the six regions in Fig. 6, as discussed in detail below.

447 BC annual mean burden over the HTP has nearly equal contributions from BB and FF  
448 emissions. However, contribution by BB emissions, mainly from SAS, is larger than from FF  
449 sector in DJF and MAM. In the summer (JJA), the largest contribution (about 29%) to HTP BC  
450 is from EAS FF emissions. This is partly due to the change of circulation patterns (Fig. 4) and  
451 effective wet removal of SAS BB emissions. Note that EAS FF emissions are much larger than  
452 FF emissions from any other of the source regions, and are more than twice the EAS BB  
453 emissions.

454 For BC in the five finer receptor regions of interest (as defined in Fig. 5g), SAS BB and  
455 FF have the largest contribution to BC in Himalayas and Central Plateau, while EAS FF and BB

456 contribute the most to Northeast Plateau in all seasons and Southeast Plateau in the summer.  
457 Central Asia and Middle East FF emissions have relatively more important contribution to BC  
458 reaching Northwest Plateau, especially in the summer.

459 For the Northwest Plateau, the prevailing winds in this sub-region are westerly  
460 throughout the year (Fig. S2; Cao et al., 2009; Xu et al., 2009), so the important source regions  
461 ought to locate at the west of HTP (e.g., MDE, EUR, and parts of SAS and RBU in Fig. 1a). [As](#)  
462 [shown in Fig. 6](#), SAS emissions are still the dominant source for the annual BC burden in this  
463 sub-region (17% from BB and 14% from FF), followed by HTP local emissions (9% from BB  
464 and 13% from FF), CAS (2% from BB and 14% from FF), MDE FF (8%) and EAS FF (7%). BC  
465 emissions from SAS are the dominant source in DJF, MAM and SON. CAS becomes the  
466 dominant source region (5% from BB and 26% from FF) in JJA, even though CAS is not a  
467 significant emission source region on a global basis (Fig. 1b). BC emitted from MDE is  
468 predominantly in the FF sector throughout the year. Emissions from the rest of the tagged  
469 sources (in addition to the [six sources listed; black bar in Fig. 6](#)) become more significant in this  
470 sub-region, mostly from EUR and RBU through long-range transport (Fig. S3). The source  
471 attribution for BC deposition in this sub-region is similar to that of the column burden, but BC  
472 emitted from SAS and MDE appears to be more efficient in deposition except for the JJA season  
473 when BC from EAS contributes more to deposition than to column burden.

474 The Himalayas sub-region located along the southern edge of the HTP is in close  
475 proximity to the SAS. Thus emissions from SAS are absolutely the dominant source for BC in  
476 Himalayas throughout the year. This sub-region receives more BC from BB sector than FF  
477 because BC emissions in SAS are mainly in the BB sector, especially in MAM season (Fig. 1b  
478 and Fig. S6). For the annual mean burden, BC from SAS contributes 81% (54% from BB and

HW 5/18/2015 11:06 AM

Deleted: (Fig. 6b),

HW 5/18/2015 11:06 AM

Deleted: top

HW 5/18/2015 11:06 AM

Deleted: (black color in Fig. 6b),

482 27% from FF), followed by HTP local emissions (6% from BB and 3% from FF). It is worth  
483 noting that SAF BB emissions contribute about 10% to burden in DJF through a long-range  
484 transport. BC deposition in this sub-region also predominantly originates from SAS, which is  
485 consistent with previous studies by Ming et al. (2008) and Kopacz et al. (2011).

486 For the Southeast Plateau (Fig. 6), the BC source contribution profile is similar to that of  
487 Himalayas during DJF and MAM season, in which SAS is still the dominant source, especially  
488 in MAM (74% contribution to column burden, including 53% from BB and 21% from FF),  
489 although the contribution from EAS is larger here than for the Himalayas. As also pointed by  
490 Ramanathan et al. (2007), BC over the SAS can be transported to the Southeast Plateau by the  
491 southern branch of the westerlies during the winter and spring. However, the BC source  
492 contribution profile changes dramatically during the summer when emissions in EAS become the  
493 dominant source to this sub-region (68% to column burden, including 23% from BB and 45%  
494 from FF). Kopacz et al. (2011) also found that the BC from south-eastern China is the dominant  
495 contributor to the Southeast Plateau in July. For the annual mean burden in this sub-region, SAS  
496 is still the dominant contributor (40% from BB and 17% from FF), followed by EAS (8% from  
497 BB and 15% from FF), HTP (6% from BB and 6% from FF). BC originating from EAS  
498 contributes more to deposition than to burden in this sub-region.

499 For the Central Plateau (Fig. 6), source attribution profiles for annual and seasonal BC  
500 are very similar to those of the entire HTP region with SAS being the dominant source region  
501 throughout the year except that EAS has comparable contributions in JJA. Ming et al. (2010)  
502 pointed out that pollutants from the Indo-Gangetic Basin could be transported to the Central  
503 Plateau by both the summer monsoon and the westerlies. Xia et al. (2011) also found that the  
504 substantial regional atmospheric brown haze from the nearby regions of SAS is the main source

HW 5/18/2015 11:06 AM

Deleted: 6d

HW 5/18/2015 11:06 AM

Deleted: 6e

507 for the background aerosols in the Central Plateau based on sunphotometer and satellite  
508 observations.

509 Compared to the other sub-regions, the Northeast Plateau receives the largest contribution  
510 of BC from EAS throughout the year (50% to annual mean burden, including 12% from BB and  
511 38% from FF; see Fig. 6), especially in JJA (17% from BB and 49% from FF). The EAS FF  
512 sector contribution and the magnitude of burden (Fig. 5f) over the Northeast Plateau have strong  
513 seasonal variations, mostly due to variations in meteorology because the FF emissions in our  
514 simulation do not vary seasonally. Kopacz et al. (2011) indicate that the primary contribution to  
515 BC over the Northeast Plateau is from western China during January and April (transported by  
516 mid-tropospheric westerlies), and from central-eastern China during July and October  
517 (transported by boundary layer flow). Other main contributions to BC burden over the Northeast  
518 Plateau include 13% from SAS and 10% from HTP local emissions. Similar to the Northwest  
519 Plateau, some other upwind source regions (e.g., CAS, MDE, RBU and EUR; see Figs. 4 and S3)  
520 have a significant contribution to the Northeast sub-region as well.

#### 521 4.4 Seasonal variation of HTP BC sensitivity

522 Following Wang et al. (2014), we defined the “efficiency” metric in Sect. 2.2 to quantify the  
523 sensitivity of BC response to absolute change (e.g., per unit perturbation) of emissions in  
524 different source regions. This metric has the value of 1 if the entire globe is treated as a single  
525 source region, so we may assume the global mean efficiency of 1 as a reference to measure the  
526 sensitivity to perturbation from different source regions/sectors.

527 Figure 7 shows efficiencies of tagged sources in affecting the BC seasonal and annual  
528 mean column burden and deposition in the HTP and five sub-regions (as defined in Fig. 5g). BC

HW 5/18/2015 11:06 AM

Deleted: 6f

530 in the same receptor regions is generally most sensitive to change in local emissions, regardless  
531 of seasons, emission sectors and locations of receptor regions. Among all the source regions,  
532 although the HTP local (FF+BB) emissions only contribute about 10%, BC in the HTP is  
533 extremely sensitive to changes in the emissions within HTP (not shown in the figure), mainly  
534 because the emission rate is very low. In addition to the local emissions, BC in the HTP is also  
535 sensitive to emissions in neighboring source regions (e.g., SAS and CAS) and emissions from  
536 distant sources such as MDE. Not only does the SAS have large contribution to BC burden and  
537 deposition over the HTP, as well as most of the sub-regions except for the Northeast Plateau  
538 (receptor V), but also the efficiencies for SAS emissions are high for almost all of the sub-  
539 regions especially the Himalayas (receptor II). BC in the Northeast Plateau (receptor V) is quite  
540 sensitive to EAS emissions in all seasons, while BC in the Southeast Plateau is sensitive to EAS  
541 emissions in JJA and SON. Although BC emissions from MDE and CAS are weak (Fig. 1b) and  
542 their contributions to the HTP are relatively low, their efficiencies are high. BC over Northwest  
543 Plateau (receptor I) and Central Plateau (receptor IV) is extremely sensitive to emissions from  
544 CAS in JJA. These source-receptor relationships of sensitivity will provide useful information  
545 for policymakers to improve the effective mitigation road map in order to potentially slow down  
546 the glacier retreat in the HTP region.

547

## 548 **5 Radiative forcing**

549 The BC-in-snow effect can be quantified using the online calculation of radiative forcing in the  
550 SNICAR (Snow, Ice, and Aerosol Radiative) model (Flanner et al., 2007) coupled to CAM5, and  
551 then compared to airborne BC radiative forcing. Figure 8 shows seasonal and annual mean BC

552 all-sky shortwave direct radiative forcing (DRF) at the surface (dimming) and the top of the  
553 atmosphere (TOA), and the BC-in-snow radiative forcing (darkening) averaged over the entire  
554 HTP and the five sub-regions (as defined in Fig. 5g). Note that the BC-in-snow forcing is  
555 averaged over all model grids in the area (i.e., zero enters the calculation for any grid when snow  
556 is not present). The radiative forcing of BC (and dust) in snow is small in JJA and SON due to a  
557 lack of snow cover (Fig. 3). The forcing maximum occurs during the spring melt (MAM) when  
558 the insolation is rather intense and BC accumulates at the surface of the snowpack as the snow  
559 melts (Conway et al., 1996; Flanner et al., 2007, 2009), and when the snow-albedo feedback is  
560 strongest (Hall and Qu, 2006). This strong seasonal variation also explains why the coefficient of  
561 variation (i.e., the ratio of the SD to the mean) is greater than 1 for the annual mean BC-in-snow  
562 forcing over the entire HTP and all sub-regions. The seasonal variations of airborne BC DRF at  
563 the TOA and surface are consistent with that of the BC column burden (Fig. 5). For the entire  
564 HTP (Fig. 8a1), the annual mean surface radiative forcing due to BC in snow ( $0.42 \text{ W m}^{-2}$ )  
565 exceeds the BC dimming effect at the surface ( $-0.3 \text{ W m}^{-2}$ ). The annual mean BC-in-snow  
566 forcing is even higher over the Northwest Plateau (Fig. 8b1) and Himalayas (Fig. 8c1), and far  
567 exceeds the other forcings in the same sub-regions, although the BC-in-snow effect may be  
568 overestimated due to the potential positive bias in snow cover fraction in our simulation (Fig. 3).  
569 The annual mean BC surface dimming exceeds the BC-in-snow effect in the Southeast (Fig. 8d1),  
570 Central (Fig. 8e1) and Northeast Plateau (Fig. 8f1). The minima of all BC-related forcings  
571 appear in the Central Plateau where the BC burden and deposition are the lowest among all the  
572 sub-regions (Fig. 5), and the SCF is very small (Fig. 3).

573 We have also calculated an approximate source attribution for the BC-in-snow radiative  
574 forcing over the HTP and its sub-regions, using the tagged-source BC deposition, which is



575 simply assumed to be linearly proportional to BC-in-snow radiative forcing. The SCF is taken  
576 into account in the calculation (i.e., the deposition at each model grid is multiplied by SCF when  
577 calculating the area-average deposition). Overall, despite small quantitative differences, the  
578 source contributions to BC-in-snow forcing are similar to those for BC deposition (Fig. 6). The  
579 SAS BB emissions contribute the most to annual mean forcing over the HTP and sub-regions  
580 except for the Northeast Plateau that is mostly contributed by EAS FF emissions. During the  
581 winter and spring seasons over Northwest Plateau and Himalayas, when and where the forcing is  
582 the largest, SAS (especially the BB sector) is the major contributor.

583 Dust is a major contributor to the total aerosol burden over the HTP (e.g., Zhang et al.,  
584 2001). Although we don't focus on other snow impurities such as mineral dust, it is worth noting  
585 that dust-in-snow radiative forcing has been considered in our model simulation and it could be  
586 an important forcing agent. We also plotted dust-in-snow forcing over the HTP and sub-regions  
587 in Fig. 8 (along with the BC-induced forcings). The annual mean dust-in-snow forcing ( $0.33 \text{ W}$   
588  $\text{m}^{-2}$ ) is comparable to all of the other forcings over the HTP, especially in the springtime when  
589 dust outbreaks and can be transported to the HTP from the surrounding sources such as  
590 Taklimakan and Gobi deserts (Liu et al., 2008). The annual mean dust-in-snow forcing is as large  
591 as  $0.99$  and  $0.59 \text{ W m}^{-2}$  in the Northwest and Northeast Plateau, respectively (Fig. 8b1 and f1),  
592 which is in close proximity to the Taklimakan Desert (Huang et al., 2007; Chen et al., 2013), but  
593 negligibly small in the Southeast Plateau and Central Plateau. In the winter, the dominant dust in  
594 snow effect over Northeast Plateau is consistent with the recent observations. Huang et al. (2011),  
595 X. Wang et al. (2013) and Zhang et al. (2013) found that insoluble light-absorbing particles in  
596 snow are dominated by local soil and desert dust in the Qilian Mountain (Northeast Plateau).

597 Both snow cover fraction (SCF) and mass concentration of snow impurities affect the  
598 calculation of radiative forcing in snow. We have evaluated the model estimation of SCF in  
599 different seasons (Fig. 3). We have also compared BC concentration and deposition flux from  
600 our model results to a recent modeling study by Ménégóz et al. (2014) and to observations in the  
601 HTP (Ginot et al., 2014) (Table S3). Bond et al. (2013) pointed out that observations of BC in  
602 snow pits or ice cores mostly involve snow/ice samples obtained in the summer and early fall,  
603 when almost all grid boxes the sample sites located in are snow free in the HTP. They also  
604 indicated that the CAM3 global climate model (Flanner et al., 2009) may be overestimating snow  
605 BC concentrations in the HTP, especially in the spring. Our comparison shows that despite a  
606 smaller bias than in Ménégóz et al. (2014) the CAM5 model still largely overestimates BC  
607 concentrations in snow but underestimates dust concentrations in snow over the HTP. Ménégóz  
608 et al. (2014) provided a few possible reasons for the differences between model simulations and  
609 observations. Factors such as measurement uncertainties (due to sample treatment and analysis  
610 methodology), temporal (inter-annual and seasonal) and spatial variations of BC deposition, and  
611 vertical variations of BC in snowpack, can strongly affect the accuracy and representativeness of  
612 BC-in-snow measurements for the purpose of evaluating global models. Ming et al. (2013) and  
613 Qian et al. (2015) pointed out that BC concentrations in snow and ice samples over HTP tend to  
614 decrease with increasing glacier elevations, while global models with coarse grid resolution  
615 cannot accurately represent elevation of sampling sites. Often times the difference is significant.  
616 Nonetheless, it is likely that positive biases exist in the modeled concentration and radiative  
617 forcing of BC and dust in snow.

## 618 **6 Summary and conclusions**

619 In this study, we employed the CAM5 model with a newly developed source tagging technique,  
620 nudged towards the MERRA meteorological reanalysis, to characterize the fate of BC particles  
621 emitted from various geographical regions and sectors to the HTP region. In addition, we  
622 compare the radiative forcing induced by BC in the atmosphere and in snow over the HTP, as  
623 well as forcing induced by dust in snow. Although there are biases in the simulated BC, partly  
624 due to the inherent difficulty for coarse-resolution global models to accurately represent transport  
625 and wet deposition in this topographically complex region, the CAM5 model simulation shows a  
626 reasonable agreement in the seasonal variation of the near-surface airborne BC concentrations  
627 with observations over the HTP and surrounding regions. This provides us the confidence to use  
628 this modeling framework to characterize BC source-receptor relationships in the HTP. Using  
629 very different approaches, Kopacz et al. (2011), Lu et al. (2012) and the present study all show  
630 that South Asia and East Asia are the main source regions for BC transported to the HTP, while  
631 the magnitude of contributions from each of the source regions varies with season and receptor  
632 location. Although all of the three studies can provide quantitative source attributions, a  
633 quantitative inter-comparison of the findings is quite difficult, given the differences in the  
634 definition of geographical source and receptor regions, emission inventories, time periods for  
635 model simulation, and analysis methods. Nevertheless, in addition to quantifying the  
636 contributions of source regions, our direct source tagging approach allows us to further break  
637 down regional contributions by sectors (i.e., fossil fuel vs. biomass & biofuel) and to characterize  
638 the transport pathways of individual regional/sectoral emissions.

639 The explicit source tagging technique enables the characterization of three-dimensional  
640 transport pathways of BC to the HTP from different geographical regions and source sectors,  
641 which also depends on seasons and the location of the receptor in the HTP. With the IPCC AR5

642 present-day emission inventories, the annual mean BC column burden and surface deposition in  
643 the entire HTP region is contributed the most by biomass and biofuel (BB) emissions from South  
644 Asia (SAS) (33% and 40%, respectively), followed by fossil fuel (FF) emissions from SAS (17%  
645 and 20%, respectively), and then the FF from East Asia (EAS) (14% and 14%, respectively). The  
646 same roles hold for all the seasonal means except for the summer when the EAS FF becomes  
647 more important. Although BC emissions from the entire EAS source region are much stronger  
648 than those from SAS, the concentrated FF BC emissions in central-eastern China are only  
649 transported towards the HTP during the East Asian summer monsoon. Thus seasonal prevailing  
650 winds are important in determining the seasonal variations in BC transport and source-receptor  
651 relationships.

652 Both the annual and seasonal mean BC properties and their source-receptor relationships  
653 vary significantly with location in the HTP. For the multiple finer receptor regions of interest,  
654 SAS BB and FF have the largest impact on BC in Himalayas and Central Plateau, while EAS FF  
655 and BB contribute the most to Northeast Plateau in all seasons and Southeast Plateau in the  
656 summer. The Central Asia (CAS) and Middle East (MDE) FF emissions make important  
657 contributions to BC over the Northwest Plateau, especially from CAS in JJA.

658 The HTP BC is most sensitive by far to per unit changes in the local emissions, although  
659 they only contribute about 10% to the BC burden in the HTP. The SAS region makes large  
660 contributions to BC burden and deposition over the HTP and the BC sensitivities to SAS  
661 emissions are also high for almost all of the sub-regions of HTP, especially the Himalayas. BC  
662 over the Northeast Plateau is quite sensitive to EAS emissions in all seasons, and Southeast  
663 Plateau BC is also sensitive to EAS emissions in JJA. Although BC emissions from MDE and  
664 CAS are weak and their contribution to the HTP overall is low, their efficiencies are quite high.

665 BC over Northwest Plateau and Central Plateau is extremely sensitive to emissions from CAS in  
666 JJA. These source-receptor relationships and sensitivities can be useful to policymakers for  
667 improving the effective mitigation road map in order to potentially slow down the glacier retreat  
668 in the HTP region.

669 The impact of BC on snow and glacier melting can be characterized by the magnitude of  
670 radiative forcing. Our calculations show that the annual mean BC-in-snow radiative forcing ( $0.42$   
671  $W m^{-2}$ ) outweighs BC dimming effect ( $-0.3 W m^{-2}$ ) at the surface over the HTP. In the five sub-  
672 regions, the annual mean BC-in-snow forcing ranges from  $0.04 W m^{-2}$  in the Central Plateau to  
673  $1.75 W m^{-2}$  in the Northwest Plateau. We also showed that the annual mean dust-in-snow  
674 induced radiative forcing over the HTP can be quite significant ( $0.33 W m^{-2}$  for entire the HTP,  
675 and  $0.99 W m^{-2}$  for the Northwest Plateau). More importantly, both BC- and dust-in-snow  
676 forcing peaks in the spring melting season when the area-average forcing reaches  $1.03$  and  $0.87$   
677  $W m^{-2}$ , respectively, over the entire HTP, and their combined forcing is more than  $8 W m^{-2}$  over  
678 the Northwest Plateau. Such a large forcing is sufficient to cause earlier snow melting and  
679 contribute to the acceleration of glacier retreat, although the model is likely to overestimate BC-  
680 in-snow forcing due to the possible positive bias of snow cover fraction in the winter and early  
681 spring. According to our estimates of the source attribution, the biomass burning and biofuel  
682 emissions in South Asia contribute the most to annual mean forcing over the HTP and its sub-  
683 regions except for the Northeast Plateau where the largest contribution is from East Asia fossil  
684 fuel emissions. During the winter and spring seasons over Northwest Plateau and Himalayas,  
685 when and where the forcing is the largest, South Asia (especially the biomass burning and  
686 biofuel sector) is the major contributor.

687

688 *Acknowledgments.* This research is based on work supported by the U.S. Department of Energy (DOE),  
689 Office of Science, Biological and Environmental Research as part of the Earth System Modeling  
690 Program. The Pacific Northwest National Laboratory (PNNL) is operated for DOE by Battelle Memorial  
691 Institute under contract DE-AC05-76RLO1830. The CESM project is supported by the National Science  
692 Foundation and the DOE Office of Science. R. Zhang acknowledges support from the China Scholarship  
693 Fund. J. Huang and Q. Fu acknowledge support from the National Basic Research Program of China  
694 (2012CB955303), NSFC grant 41275070 and China 111 project (No. B13045). Computational resources  
695 were provided by the National Energy Research Scientific Computing Center (NERSC), a national  
696 scientific user facility located at Lawrence Berkeley National Laboratory in Berkeley, California. NERSC  
697 is the flagship scientific computing facility for the Office of Science in DOE.

698

## 699 **References**

- 700 Babu, S. S., Chaubey, J. P., Moorthy, K. K., Gogoi, M. M., Kompalli, S. K., Sreekanth, V., Bagare, S. P., Bhatt, B.  
701 C., Gaur, V. K., Prabhu, T. P., and Singh, N. S.: High altitude (~4520 m amsl) measurements of black  
702 carbon aerosols over western trans-Himalayas: Seasonal heterogeneity and source apportionment, *J.*  
703 *Geophys. Res.*, 116, D24201, doi:10.1029/2011JD016722, 2011.
- 704 Barnett, T. P., Adam, J. C., and Lettenmaier, D. P.: Potential impacts of a warming climate on water availability in  
705 snow-dominated regions, *Nature*, 438, 303–309, doi:10.1038/Nature04141, 2005.
- 706 Bolch, T., Kulkarni, A., Kääb, A., Huggel, C., Paul, F., Cogley, J., Frey, H., Kargel, J., Fujita, K., Scheel, M.,  
707 Bajracharya, S., and Stoffel, M.: The state and fate of Himalayan Glaciers, *Science*, 336, 310–314,  
708 doi:0.1126/science.1215828, 2012.
- 709 Bond, T. C., Bhardwaj, E., Dong, R., Jogani, R., Jung, S., Roden, C., Streets, D. G., and Trautmann, N. M.:  
710 Historical emissions of black and organic carbon aerosol from energy-related combustion, 1850–2000,  
711 *Global Biogeochem. Cy.*, 21, GB2018, doi:10.1029/2006GB002840, 2007.
- 712 Bond, T. C., Doherty, S. J., Fahey, D. W., Forster, P. M., Berntsen, T., DeAngelo, B. J., Flanner, M. G., Ghan, S.,  
713 Kärcher, B., Koch, D., Kinne, S., Kondo, Y., Quinn, P. K., Sarofim, M. C., Schultz, M. G., Schulz, M.,  
714 Venkataraman, C., Zhang, H., Zhang, S., Bellouin, N., Guttikunda, S. K., Hopke, P. K., Jacobson, M. Z.,  
715 Kaiser, J. W., Klimont, Z., Lohmann, U., Schwarz, J. P., Shindell, D., Storelvmo, T., Warren, S. G., and  
716 Zender, C. S.: Bounding the role of black carbon in the climate system: A scientific assessment, *J. Geophys.*  
717 *Res.-Atmos.*, 118, 5380–5552, doi:10.1002/jgrd.50171, 2013.
- 718 Bonasoni, P., Laj, P., Marinoni, A., Sprenger, M., Angelini, F., Arduini, J., Bonafè, U., Calzolari, F., Colombo, T.,  
719 Decesari, S., DiBiagio, C., di Sarra, A. G., Evangelisti, F., Duchi, R., Facchini, MC., Fuzzi, S., Gobbi, G. P.,  
720 Maione, M., Panday, A., Roccatò, F., Sellegri, K., Venzac, H., Verza, GP., Villani, P., Vuillermoz, E., and  
721 Cristofanelli, P.: Atmospheric Brown Clouds in the Himalayas: first two years of continuous observations  
722 at the Nepal Climate Observatory-Pyramid (5079 m), *Atmos. Chem. Phys.*, 10, 7515–7531,  
723 doi:10.5194/acp-10-7515-2010, 2010.

- 724 Cao, J. J., Xu, B. Q., He, J. Q., Liu, X. Q., Han, Y. M., Wang, G. H., and Zhu, C. S.: Concentrations, seasonal  
725 variations, and transport of carbonaceous aerosol at a remote Mountainous region in western China, *Atmos.*  
726 *Environ.*, 43, 4444–4452, doi:10.1016/j.atmosenv.2009.06.023, 2009.
- 727 Chen, S., J. Huang, C. Zhao, Y. Qian, L. R. Leung, and B. Yang: Modeling the Transport and Radiative Forcing of  
728 Taklimakan Dust over the Tibetan Plateau in Summer, *J. Geophys. Res.*, 118, 797–812,  
729 doi:10.1002/jgrd.50122, 2013.
- 730 Conway, H., Gades, A., and Raymond, C. F.: Albedo of dirty snow during conditions of melt, *Water Resour. Res.*,  
731 32, 1713–1718, doi:10.1029/96WR00712, 1996.
- 732 Dentener, F., Kinne, S., Bond, T., Boucher, O., Cofala, J., Generoso, S., Ginoux, P., Gong, S., Hoelzemann, J. J., Ito,  
733 A., Marelli, L., Penner, J. E., Putaud, J.-P., Textor, C., Schulz, M., van der Werf, G. R., and Wilson, J.:  
734 Emissions of primary aerosol and precursor gases in the years 2000 and 1750 prescribed data-sets for  
735 AeroCom, *Atmos. Chem. Phys.*, 6, 4321–4344, doi:10.5194/acp-6-4321-2006, 2006.
- 736 Doherty, S. J., Dang, C., Hegg, D. A., Zhang, R., and Warren, S. G.: Black carbon and other light-absorbing  
737 particles in snow of central North America, *J. Geophys. Res. Atmos.*, 119, 12,807–12,831,  
738 doi:10.1002/2014JD022350, 2014.
- 739 Duan, A., Wu G., Zhang Q., and Liu Y.: New proofs of the recent climate warming over the Tibetan Plateau as a  
740 result of the increasing greenhouse gases emissions, *Chin. Sci. Bull.*, 51, 1396–1400, doi:10.1007/s11434-  
741 006-1396-6, 2006.
- 742 Duan, A. M. and Wu G. X.: Weakening trend in the atmospheric heat source over the Tibetan Plateau during recent  
743 decades. Part I: Observations, *J. Clim.*, 21, 3149–3164, doi:10.1175/2007JCLI1912.1, 2008.
- 744 Flanner, M. G., Zender, C. S., Randerson, J. T., and Rasch, P. J.: Present day climate forcing and response from  
745 black carbon in snow, *J. Geophys. Res.*, 112, D11202, doi:10.1029/2006JD008003, 2007.
- 746 Flanner, M. G., Zender, C. S., Hess, P. G., Mahowald, N. M., Painter, T. H., Ramanathan, V., and Rasch, P. J.:  
747 Springtime warming and reduced snow cover from carbonaceous particles, *Atmos. Chem. Phys.*, 9, 2481–  
748 2497, doi:10.5194/acp-9-2481-2009, 2009.
- 749 Gettelman, A., Liu, X., Ghan, S. J., Morrison, H., Park, S., Conley, A. J., Klein, S. A., Boyle, J., Mitchell, D. L., and  
750 Li, J. L. F.: Global simulations of ice nucleation and ice supersaturation with an improved cloud scheme in  
751 the Community Atmosphere Model, *J. Geophys. Res.*, 115, D18216, doi:10.1029/2009jd013797, 2010.
- 752 Ginot, P., Dumont, M., Lim, S., Patris, N., Taupin, J.-D., Wagnon, P., Gilbert, A., Arnaud, Y., Marinoni, A.,  
753 Bonasoni, P., and Laj, P.: A 10 year record of black carbon and dust from a Mera Peak ice core (Nepal):  
754 variability and potential impact on melting of Himalayan glaciers, *The Cryosphere*, 8, 1479–1496,  
755 doi:10.5194/tc-8-1479-2014, 2014.
- 756 Hadley, O. L. and Kirchstetter, T.W.: Black-carbon reduction of snow albedo, *Nat. Clim. Change*, 2, 437–440, 2012.
- 757 Hall, D. K., Riggs G. A., and Salomonson V. V.: updated monthly. MODIS/TERRA Snow Cover Monthly L3  
758 Global 0.05Deg CMG V005, [2001], Boulder, CO, National Snow and Ice Data Center. Digital Media,  
759 distributed in netCDF format by the Integrated Climate Data Center (ICDC, <http://icdc.zmaw.de> University  
760 of Hamburg, Hamburg, Germany), 2006.
- 761 Hall, A. and Qu, X.: Using the current seasonal cycle to constrain snow albedo feedback in future climate change,  
762 *Geophys. Res. Lett.*, 33, L03502, doi:10.1029/2005GL025127, 2006.

- 763 Hansen, J. and Nazarenko, L.: Soot climate forcing via snow and ice albedos, *P. Natl. Acad. Sci. USA*, 101, 423–  
764 428, doi:10.1073/pnas.2237157100, 2004.
- 765 Hansen, J., Sato, M., Ruedy, R., Nazarenko, L., Lacis, A., Schmidt, G. A., Russell, G., Aleinov, I., Bauer, M., Bauer,  
766 S., Bell, N., Cairns, B., Canuto, V., Chandler, M., Cheng, Y., Del Genio, A., Faluvegi, G., Fleming, E.,  
767 Friend, A., Hall, T., Jackman, C., Kelley, M., Kiang, N., Koch, D., Lean, J., Lerner, J., Lo, K., Menon, S.,  
768 Miller, R., Minnis, P., Novakov, T., Oinas, V., Perlwitz, Ja., Perlwitz, Ju., Rind, D., Romanou, A., Shindell,  
769 D., Stone, P., Sun, S., Tausnev, N., Thresher, D., Wielicki, B., Wong, T., Yao, M., and Zhang, S.: Efficacy  
770 of climate forcings, *J. Geophys. Res.*, 110, D18104, doi:10.1029/2005JD005776, 2005.
- 771 Huang, J., Minnis, P., Yi, Y., Tang, Q., Wang, X., Hu, Y., Liu, Z., Ayers, K., Trepte, C., and Winker, D.: Summer  
772 dust aerosols detected from CALIPSO over the Tibetan Plateau, *Geophys. Res. Lett.*, 34, L18805,  
773 doi:10.1029/2007GL029938, 2007.
- 774 Huang, J., Fu, Q., Zhang, W., Wang, X., Zhang, R., Ye, H., and Warren, S. G.: Dust and black carbon in seasonal  
775 snow across Northern China, *Bull. Am. Meteorol. Soc.*, 92, 175–181, doi:10.1175/2010BAMS3064.1, 2011.
- 776 Hurrell, J. W., Holland, M. M., Ghan, S., Lamarque, J.-F., Lawrence, D., Lipscomb, W. H., Mahowald, N., Marsh,  
777 D., Rasch, P., Bader, D., Collins, W. D., Gent, P. R., Hack, J. J., Kiehl, J., Kushner, P., Large, W. G.,  
778 Marshall, S., Vavrus, S., and Vertenstein, M.: The Community Earth System Model: A Framework for  
779 Collaborative Research, *Bull. Am. Meteorol. Soc.*, 94, 1339-1360, doi:10.1175/BAMS-D-12-00121, 2013.
- 780 Immerzeel, W., VanBeek L. P. H., and Bierkens, M. F. P.: Climate Change Will Affect the Asian Water Towers,  
781 *Science*, 328, 1382–1385, doi:10.1126/science.1183188, 2010.
- 782 Jacobson, M. Z.: Climate response of fossil fuel and biofuel soot, accounting for soot’s feedback to snow and sea ice  
783 albedo and emissivity, *J. Geophys. Res.*, 109, D21201, doi:10.1029/2004JD004945, 2004.
- 784 Jiao, C., Flanner, M. G., Balkanski, Y., Bauer, S. E., Bellouin, N., Bernsten, T. K., Bian, H., Carslaw, K. S.,  
785 Chin, M., De Luca, N., Diehl, T., Ghan, S. J., Iversen, T., Kirkevåg, A., Koch, D., Liu, X., Mann, G. W.,  
786 Penner, J. E., Pitari, G., Schulz, M., Seland, Ø., Skeie, R. B., Steenrod, S. D., Stier, P., Takemura, T.,  
787 Tsigaridis, K., van Noije, T., Yun, Y., and Zhang, K.: An AeroCom assessment of black carbon in Arctic  
788 snow and sea ice, *Atmos. Chem. Phys.*, 14, 2399-2417, doi:10.5194/acp-14-2399-2014, 2014.
- 789 Kang, S., Wake C., Qin, D., Mayewski P. A., and Yao T.: Monsoon and dust signals recorded in Dasuopu glacier,  
790 Tibetan Plateau, *J. Glaciol.*, 46(153), 222–226, 2000.
- 791 Kang, S., Wei, X., You, Q., Flugel, W., Pepin, N., and Yao, T.: Review of climate and cryospheric change in the  
792 Tibetan Plateau, *Environ. Res. Lett.*, 5, 015101, doi:10.1088/1748-9326/5/1/015101, 2010.
- 793 Kaser, G., Grosshauser, M., and Marzeion, B.: Contribution of glaciers to water availability in different climate  
794 regimes, *P. Natl. Acad. Sci. USA*, 107, 20223–20227, doi:10.1073/pnas.1008162107, 2010
- 795 Kaspari, S. D., Schwikowski, M., Gysel, M., Flanner, M. G., Kang, S., Hou, S., and Mayewski, P. A.: Resent  
796 increase in black carbon concentrations from a Mt. Everest ice core spanning 1860–2000 AD, *Geophys.*  
797 *Res. Lett.*, 38, L04703, doi:10.1029/2010GL046096, 2011.
- 798 Kopacz, M., Mauzerall, D. L., Wang, J., Leibensperger, E. M., Henze, D. K., and Singh, K.: Origin and radiative  
799 forcing of black carbon transported to the Himalayas and Tibetan Plateau, *Atmos. Chem. Phys.*, 11, 2837-  
800 2852, doi:10.5194/acp-11-2837-2011, 2011.



801 Lamarque, J.-F., Bond, T. C., Eyring, V., Granier, C., Heil, A., Klimont, Z., Lee, D., Liousse, C., Mieville, A.,  
802 Owen, B., Schultz, M. G., Shindell, D., Smith, S. J., Stehfest, E., Van Aardenne, J., Cooper, O. R.,  
803 Kainuma, M., Mahowald, N., McConnell, J. R., Naik, V., Riahi, K., and van Vuuren, D. P.: Historical  
804 (1850–2000) gridded anthropogenic and biomass burning emissions of reactive gases and aerosols:  
805 methodology and application, *Atmos. Chem. Phys.*, 10, 7017–7039, doi:10.5194/acp-10-7017-2010, 2010.

806 Lamarque, J. F., Emmons, L. K., Hess, P. G., Kinnison, D. E., Tilmes, S., Vitt, F., Heald, C. L., Holland, E. A.,  
807 Lauritzen, P. H., Neu, J., Orlando, J. J., Rasch, P. J., and Tyndall, G. K.: CAM-chem: description and  
808 evaluation of interactive atmospheric chemistry in the Community Earth System Model, *Geosci. Model  
809 Dev.*, 5, 369–411, doi:10.5194/gmd-5-369-2012, 2012.

810 Lau, K. M., Kim, M. K., and Kim, K. M.: Asian monsoon anomalies induced by aerosol direct forcing: the role of  
811 the Tibetan Plateau, *Clim. Dyn.*, 26, 855–664, 2006.

812 Lau, K.-M., Kim, M. K., Kim, K.-M., and Lee, W. S.: Enhanced surface warming and accelerated snow melt in the  
813 Himalayas and Tibetan Plateau induced by absorbing aerosols, *Environ. Res. Lett.*, 5, 025204  
814 doi:10.1088/1748-9326/5/2/025204, 2010.

815 Lee, Y. H., Lamarque, J.-F., Flanner, M. G., Jiao, C., Shindell, D. T., Berntsen, T., Bisiaux, M. M., Cao, J.,  
816 Collins, W. J., Curran, M., Edwards, R., Faluvegi, G., Ghan, S., Horowitz, L. W., McConnell, J. R.,  
817 Ming, J., Myhre, G., Nagashima, T., Naik, V., Rumbold, S. T., Skeie, R. B., Sudo, K., Takemura, T.,  
818 Thevenon, F., Xu, B., and Yoon, J.-H.: Evaluation of preindustrial to present-day black carbon and its  
819 albedo forcing from Atmospheric Chemistry and Climate Model Intercomparison Project (ACCMIP),  
820 *Atmos. Chem. Phys.*, 13, 2607–2634, doi:10.5194/acp-13-2607-2013, 2013.

821 Li, X., Cheng, G., Jin, H., Kang, E., Che, T., Jin, R., Wu, L., Nan, Z., Wang, J., and Shen, Y.: Cryospheric change in  
822 China, *Global Planet. Change*, 62(3–4), 210–218, 2008.

823 Liu, X., Easter, R. C., Ghan, S. J., Zaveri, R., Rasch, P., Shi, X., Lamarque, J.-F., Gettelman, A., Morrison, H., Vitt,  
824 F., Conley, A., Park, S., Neale, R., Hannay, C., Ekman, A. M. L., Hess, P., Mahowald, N., Collins, W.,  
825 Iacono, M. J., Bretherton, C. S., Flanner, M. G., and Mitchell, D.: Toward a minimal representation of  
826 aerosols in climate models: description and evaluation in the Community Atmosphere Model CAM5,  
827 *Geosci. Model Dev.*, 5, 709–739, doi:10.5194/gmd-5-709-2012, 2012.

828 Liu, Z., Liu, D., Huang, J., Vaughan, M., Uno, I., Sugimoto, N., Kittaka, C., Trepte, C., Wang, Z., Hostetler, C., and  
829 Winker, D.: Airborne dust distributions over the Tibetan Plateau and surrounding areas derived from the  
830 first year of CALIPSO lidar observations, *Atmos. Chem. Phys.*, 8, 5045–5060, doi:10.5194/acp-8-5045-  
831 2008, 2008.

832 Lu, Z., Streets, D. G., Zhang, Q., and Wang, S.: A novel back-trajectory analysis of the origin of black carbon  
833 transported to the Himalayas and Tibetan Plateau during 1996–2010, *Geophys. Res. Lett.*, 39, L01809,  
834 doi:10.1029/2011GL049903, 2012.

835 Ma, P.-L., Rasch, P. J., Wang, H., Zhang, K., Easter, R. C., Tilmes, S., Fast, J. D., Liu, X., Yoon, J.-H., and  
836 Lamarque, J.-F.: The role of circulation features on black carbon transport into the Arctic in the  
837 Community Atmosphere Model Version 5 (CAM5), *J. Geophys. Res. - Atmos.*, 118, 4657–4669, 2013.

838 Manabe, S., and Terpstra T. B.: The effects of mountains on the general circulation of the atmosphere as identified  
839 by numerical experiments, *J. Atmos. Sci.*, 31, 3–42, 1974.

- 840 Marinoni, A., Cristofanelli, P., Laj, P., Duchi, R., Calzolari, F., Decesari, S., Sellegri, K., Vuillermoz, E., Verza, G.  
841 P., Villani, P., and Bonasoni, P.: Aerosol mass and black carbon concentrations, a two year record at NCO-  
842 P (5079 m, Southern Himalayas), *Atmos. Chem. Phys.*, 10, 8551–8562, doi:10.5194/acp-10-8551-2010,  
843 2010.
- 844 Marinoni, A., Cristofanelli, P., Laj, P., Duchi, R., Putero, D., Calzolari, F., Landi, T. C., Vuillermoz, E., Maione, M.,  
845 and Bonasoni, P.: High black carbon and ozone concentrations during pollution transport in the Himalayas:  
846 Five years of continuous observations at NCO-P global GAW station, *J. Environ. Sci.*, 25, 1618–1625,  
847 doi:10.1016/S1001-0742(12)60242-3, 2013.
- 848 Ménégoz, M., Krinner, G., Balkanski, Y., Boucher, O., Cozic, A., Lim, S., Ginot, P., Laj, P., Gallée, H., Wagnon, P.,  
849 Marinoni, A., and Jacobi, H. W.: Snow cover sensitivity to black carbon deposition in the Himalayas: from  
850 atmospheric and ice core measurements to regional climate simulations, *Atmos. Chem. Phys.*, 14, 4237-  
851 4249, doi:10.5194/acp-14-4237-2014, 2014.
- 852 Menon, S., Koch, D., Beig, G., Sahu, S., Fasullo, J., and Orlikowski, D.: Black carbon aerosols and the third polar  
853 ice cap, *Atmos. Chem. Phys.*, 10, 4559–4571, doi:10.5194/acp-10-4559-2010, 2010.
- 854 Ming, J., Cachier, H., Xiao, C., Qin, D., Kang, S., Hou, S., and Xu, J.: Black carbon record based on a shallow  
855 Himalayan ice core and its climatic implications, *Atmos. Chem. Phys.*, 8, 1343–1352, doi:10.5194/acp-8-  
856 1343-2008, 2008.
- 857 Ming, J., Xiao, C. D., Cachier, H., Qin, D. H., Qin, X., Li, Z. Q., and Pu, J. C.: Black carbon (BC) in the snow of  
858 glaciers in west China and its potential effects on albedos, *Atmos. Res.*, 92, 114–123,  
859 doi:10.1016/j.atmosres.2008.09.007, 2009.
- 860 Ming, J., Xiao C., Sun J., Kang S., and Bonasoni P.: Carbonaceous particles in the atmosphere and precipitation of  
861 the Nam Co region, central Tibet, *J. Environ. Sci.*, 22(11), 1748–1756, doi:10.1016/S1001-0742(09)60315-  
862 6, 2010.
- 863 Ming, J., Xiao, C., Du, Z., and Yang, X.: An overview of black carbon deposition in High Asia glaciers and its  
864 impacts on radiation balance, *Adv. Water Resour.*, 55, 80–87, 2013.
- 865 Moorthy, K. K., Beegum, S. N., Srivastava, N., Satheesh, S. K., Chin, M., Blond, N., Babu, S. S., and Singh, S.:  
866 Performance evaluation of chemistry transport models over India, *Atmos. Environ.*, 71, 210–225, 2013.
- 867 Neale, R. B., Chen, C.-C., Gettelman, A., Lauritzen, P. H., Park, S., Williamson, D. L., Conley, A. J., Garcia, R.,  
868 Kinnison, D., Lamarque, J.-F., Marsh, D., Mills, M., Smith, A. K., Tilmes, S., Vitt, F., Cameron-Smith, P.,  
869 Collins, W. D., Iacono, M. J., Easter, R. C., Ghan, S. J., Liu, X., Rasch, P. J., and Taylor, M. A.:  
870 Description of the NCAR Community Atmosphere Model (CAM 5.0), NCAR/TN-486+STR, available at:  
871 [http://www.cesm.ucar.edu/models/cesm1.0/cam/docs/description/cam5\\_desc.pdf](http://www.cesm.ucar.edu/models/cesm1.0/cam/docs/description/cam5_desc.pdf) (last access: 26 December  
872 2014), 2012.
- 873 Ohara, T., Akimoto, H., Kurokawa, J., Horii, N., Yamaji, K., Yan, X., and Hayasaka, T.: An Asian emission  
874 inventory of anthropogenic emission sources for the period 1980–2020, *Atmos. Chem. Phys.*, 7, 4419–4444,  
875 doi:10.5194/acp-7-4419-2007, 2007.
- 876 Petzold, A., Ogren, J. A., Fiebig, M., Laj, P., Li, S.-M., Baltensperger, U., Holzer-Popp, T., Kinne, S.,  
877 Pappalardo, G., Sugimoto, N., Wehrl, C., Wiedensohler, A., and Zhang, X.-Y.: Recommendations for  
878 reporting "black carbon" measurements, *Atmos. Chem. Phys.*, 13, 8365–8379, doi:10.5194/acp-13-8365-  
879 2013, 2013.

- 880 Prasad, A. K. and Singh, R. P.: Changes in Himalayan Snow and Glacier Cover Between 1972 and 2000, *Eos Trans.*  
881 *AGU*, 88, 33, doi:10.1029/2007EO330002, 2007.
- 882 Pu, Z., Xu L., and Salomonson V. V.: MODIS/Terra observed seasonal variations of snow cover over the Tibetan  
883 Plateau, *Geophys. Res. Lett.*, 34, L06706, doi:10.1029/2007GL029262, 2007.
- 884 Qian, Y., Flanner, M. G., Leung, L. R., and Wang, W.: Sensitivity studies on the impacts of Tibetan Plateau  
885 snowpack pollution on the Asian hydrological cycle and monsoon climate, *Atmos. Chem. Phys.*, 11, 1929-  
886 1948, doi:10.5194/acp-11-1929-2011, 2011.
- 887 Qian, Y., Wang H., Zhang R., Flanner M. G., and Rasch P. J.: A sensitivity study on modeling black carbon in snow  
888 and its radiative forcing over the Arctic and Northern China, *Environ. Res. Lett.*, 9, 064001,  
889 doi:10.1088/1748-9326/9/6/064001, 2014.
- 890 Qian, Y., Yasunari, T. J., Doherty, S. J., et al., Light-absorbing particles in snow and ice: measurement and  
891 modeling of climatic and hydrological impact. *Adv. Atmos. Sci.*, 32(1), 64-91 doi: 10.1007/s00376-014-  
892 0010-0, 2015.
- 893 Qin, D., Liu, S., and Li, P.: Snow cover distribution, variability, and response to climate change in western China, *J.*  
894 *Clim.*, 19(9), 1820–1833, 2006.
- 895 Qiu, J.: China: the third pole. *Nature News*, 454(7203), 393-396, 2008.
- 896 Ram, K., Sarin, M. M., and Hegde, P.: Long-term record of aerosol optical properties and chemical composition  
897 from a high-altitude site (Manora Peak) in Central Himalaya, *Atmos. Chem. Phys.*, 10, 11791–11803,  
898 doi:10.5194/acp-10-11791-2010, 2010.
- 899 Ramanathan, V., Ramana, M. V., Roberts, G., Kim, D., Corrigan, C., Chung, C., Winker, D.: Warming trends in  
900 Asia amplified by brown clouds solar absorption, *Nature*, 448, 575–578, 2007.
- 901 Rasch, P. J., Mahowald, N. M., and Eaton, B. E.: Representations of transport, convection, and the hydrological  
902 cycle in chemical transport models: Implications for the modeling of short-lived and soluble species, *J.*  
903 *Geophys. Res.*, 102, 28 127–28 138, 1997.
- 904 Ren, J., Jing, Z., Pu, J., and Qin, X.: Glaciers variations and climate change in the central Himalaya over the past  
905 few decades, *Ann. Glaciol.*, 43, 218–222, 2006.
- 906 Rienecker, M. M., Suarez, M. J., Gelaro, R., Todling, R., Bacmeister, J., Liu, E., Bosilovich, M. G., Schubert, S. D.,  
907 Takacs, L., Kim, G.-K., Bloom, S., Chen, J., Collins, D., Conaty, A., da Silva, A., Gu, W., Joiner, J., Koster,  
908 R. D., Lucchesi, R., and Molod, A.: MERRA – NASA’s Modern-Era Retrospective Analysis for Research  
909 and Applications, *J. Clim.*, 24, 3624–3648, 2011.
- 910 Shindell, D. T., Chin, M., Dentener, F., Doherty, R. M., Faluvegi, G., Fiore, A. M., Hess, P., Koch, D. M.,  
911 MacKenzie, I. A., Sanderson, M. G., Schultz, M. G., Schulz, M., Stevenson, D. S., Teich, H., Textor, C.,  
912 Wild, O., Bergmann, D. J., Bey, I., Bian, H., Cuvelier, C., Duncan, B. N., Folberth, G., Horowitz, L. W.,  
913 Jonson, J., Kaminski, J. W., Marmer, E., Park, R., Pringle, K. J., Schroeder, S., Szopa, S., Takemura, T.,  
914 Zeng, G., Keating, T. J., and Zuber, A.: A multi-model assessment of pollution transport to the Arctic,  
915 *Atmos. Chem. Phys.*, 8, 5353-5372, doi:10.5194/acp-8-5353-2008, 2008.
- 916 Singh, P. and Bengtsson, L.: Hydrological sensitivity of a large Himalayan basin to climate change, *Hydrol. Process.*,  
917 18, 2363–2385, 2004.

- 918 Taylor, K. E., Stouffer, R. J., and Meehl, G. A.: An Overview of CMIP5 and the Experiment Design, *Bull. Am.*  
919 *Meteorol. Soc.*, 93, 485–498, doi:10.1175/BAMS-D-11-00094.1, 2012.
- 920 Wang, B., Bao, Q., Hoskins, B., Wu, G., and Liu, Y.: Tibetan Plateau warming and precipitation changes in East  
921 Asia, *Geophys. Res. Lett.*, 35, L14702, doi:10.1029/2008GL034330, 2008.
- 922 Wang, H., Easter, R. C., Rasch, P. J., Wang, M., Liu, X., Ghan, S. J., Qian, Y., Yoon, J.-H., Ma, P.-L., and Vinoj, V.:  
923 Sensitivity of remote aerosol distributions to representation of cloud–aerosol interactions in a global  
924 climate model, *Geosci. Model Dev.*, 6, 765–782, doi:10.5194/gmd-6-765-2013, 2013.
- 925 Wang, H., Rasch, P. J., Easter, R. C., Singh, B., Zhang, R., Ma, P. L., Qian, Y., and Beagley, N.: Using an explicit  
926 emission tagging method in global modeling of source-receptor relationships for black carbon in the Arctic:  
927 Variations, Sources and Transport pathways, *J. Geophys. Res.-Atmos.*, 119, 12888–12909, doi:  
928 10.1002/2014JD022297, 2014.
- 929 Wang, M., Xu, B., Cao, J., Tie, X., Wang, H., Zhang, R., Qian, Y., Rasch, P. J., Zhao, S., Wu, G., Zhao, H.,  
930 Joswiak, D. R., Li, J., and Xie, Y.: Carbonaceous aerosols recorded in a southeastern Tibetan glacier:  
931 analysis of temporal variations and model estimates of sources and radiative forcing, *Atmos. Chem. Phys.*,  
932 15, 1191–1204, doi:10.5194/acp-15-1191-2015, 2015.
- 933 Wang, X., S. J. Doherty, and J. Huang: Black carbon and other light-absorbing impurities in snow across Northern  
934 China, *J. Geophys. Res. Atmos.*, 118, 1471–1492, doi:10.1029/2012JD018291, 2013.
- 935 Warren, S. G. and Wiscombe, W. J.: A model for the spectral albedo of snow. II: Snow containing atmospheric  
936 aerosols, *J. Atmos. Sci.*, 37, 2734–2745, 1980.
- 937 Warren, S. G. and Wiscombe, W. J.: Dirty snow after nuclear war, *Nature*, 313, 469–470, 1985.
- 938 Wu, G., Liu, Y., He, B., Bao, Q., Duan, A., and Jin, F.-F.: Thermal controls on the Asian summer monsoon, *Sci.*  
939 *Rep.*, 2, 404, doi:10.1038/srep00404, 2012.
- 940 Xia, X. G., Zong, X. M., Cong, Z. Y., Chen, H. B., Kang, S. C., and Wang, P. C.: Baseline continental aerosol over  
941 the central Tibetan plateau and a case study of aerosol transport from South Asia, *Atmos. Environ.*, 45,  
942 7370–7378, 2011.
- 943 Xu, B., Cao, J., Hansen, J., Yao, T., Joswiak, D. R., Wang, N., Wu, G., Wang, M., Zhao, H., Yang, W., Liu, X., and  
944 He, J.: Black soot and the survival of Tibetan glaciers, *Proc. Natl. Acad. Sci. USA*, 106, 22114–22118,  
945 2009.
- 946 Xu, X., Lu C., Shi X., and Gao S.: World water tower: An atmospheric perspective, *Geophys. Res. Lett.*, 35, L20815,  
947 doi:10.1029/2008GL035867, 2008.
- 948 Yanai, M., Li, C., and Song, Z.: Seasonal heating of the Tibetan Plateau and its effects on the evolution of the Asian  
949 summer monsoon, *Journal of the Meteorological Society of Japan*, 70, 319–351, 1992.
- 950 Yao, T., Pu, J., Lu, A., Wang, Y., and Yu, W.: Recent glacial retreat and its impact on hydrological processes on the  
951 Tibetan Plateau, China, and surrounding regions, *Arct. Antarct. Alp. Res.*, 39(4), 642–650, 2007.
- 952 Yao, T., Thompson, L., Yang, W., Yu, W., Gao, Y., Guo, X., Yang, X., Duan, K., Zhao, H., Xu, B., Pu, J., Lu, A.,  
953 Xiang, Y., Kattel, D. B., and Joswiak, D.: Different glacier status with atmospheric circulations in Tibetan  
954 Plateau and surroundings, *Nat. Clim. Change*, 2, 663–667, doi:10.1038/nclimate1580, 2012.

- 955 Yasunari, T. J., Bonasoni, P., Laj, P., Fujita, K., Vuillermoz, E., Marinoni, A., Cristofanelli, P., Duchi, R., Tartari,  
956 G., and Lau, K.-M.: Estimated impact of black carbon deposition during premonsoon season from Nepal  
957 Climate Observatory – Pyramid data and snow albedo changes over Himalayan glaciers, *Atmos. Chem.*  
958 *Phys.*, 10, 6603–6615, doi:10.5194/acp-10-6603-2010, 2010.
- 959 Ye, D. and Gao, Y.: *Meteorology of the Qinghai-Xizang Plateau* (Chinese Science Press, Beijing, 1979).
- 960 Ye, D. and Wu G.: The role of the heat source of the Tibetan Plateau in the general circulation, *Meteorol. Atmos.*  
961 *Phys.*, 67, 181–198, doi:10.1007/BF01277509, 1998.
- 962 Ye, H., Zhang, R., Shi, J., Huang, J., Warren, S. G., and Fu, Q.: Black carbon in seasonal snow across northern  
963 Xinjiang in northwestern China, *Environ. Res. Lett.* 7, 044002, doi:10.1088/1748-9326/7/4/044002, 2012.
- 964 Yeh, T., Lo, S., and Chu P.: The wind structure and heat balance in the lower troposphere over Tibetan Plateau and  
965 its surrounding. *Acta Meteor. Sinica* 28, 108–121, 1957.
- 966 Zhang, R., Hegg, D. A., Huang, J., and Fu, Q.: Source attribution of insoluble light-absorbing particles in seasonal  
967 snow across northern China, *Atmos. Chem. Phys.*, 13, 6091-6099, doi:10.5194/acp-13-6091-2013, 2013.
- 968 Zhang, X. Y., Arimoto, R., Cao, J. J., An, Z. S., and Wang, D.: Atmospheric dust aerosol over the Tibetan Plateau, *J.*  
969 *Geophys. Res.*, 106(D16), 18 471–18 476, 2001.
- 970 Zhao, S., Ming, J., Xiao, C., Sun, W., and Qin, X.: A preliminary study on measurements of black carbon in the  
971 atmosphere of northwest Qilian Shan. *J. Environ. Sci.*, 24(1), 152-159, doi:10.1016/S1001-0742(11)60739-  
972 0, 2012.
- 973 Zhao, Z., Cao, J., Shen, Z., Xu, B., Chen, L- W. A., Ho, K., Han, Y., Zhu, C., and Liu, S.: Aerosol particles at a  
974 high-altitude site on the Southeast Tibetan Plateau, China: implications for pollution transport from South  
975 Asia, *J. Geophys. Res.-Atmos.*, 118, 11360–11375, doi:10.1002/jgrd.50599, 2013.

976

**Table 1.** List of sites for the observations of atmospheric BC surface concentrations used in this study to evaluate our model simulation.

Site	Latitude (°N)	Longitude (°E)	Elevation (m)		Sampling time	Observation method	Contributor
			observation	model			
<b>Muztagh Ata</b>	38.3	75.0	4500	3497	2003–2006	Thermal Optical Reflectance (TOR)	Cao et al., 2009
<b>Hanle</b>	32.8	79.0	4250	4862	2009–2010	Aethalometer	Babu et al., 2011
<b>Manora Peak</b>	29.4	79.5	1950	1409	2005–2008	Thermal Optical Transmittance (TOT)	Ram et al., 2010
<b>NCO-P</b>	28.0	86.8	5079	4604	2006–2008	Multi-angle absorption photometer (MAAP)	Marinoni et al., 2010
<b>Lulang</b>	29.5	94.4	3300	3370	2008–2009	TOR	Zhao et al., 2013
<b>NCOS</b>	30.8	91.0	4730	4956	2006–2007	TOR	Ming et al., 2010
<b>QSSGEE</b>	39.5	96.5	4214	2748	2009–2011	Aethalometer	Zhao et al., 2012

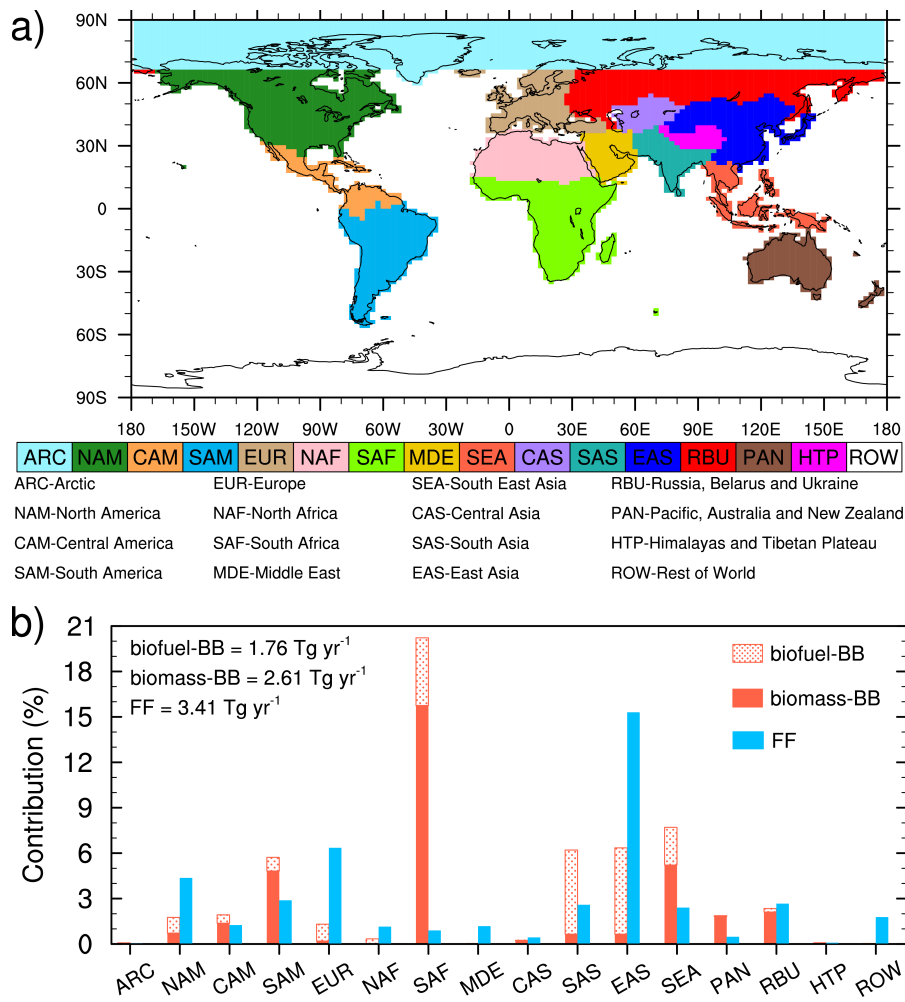


**Fig. 1.** (a) Tagged source regions and (b) the respective percentage contributions to global annual mean BC emissions from the individual source regions and sectors (including biofuel, biomass burning and fossil fuel). The global annual mean BC emission rate is  $7.78 \text{ Tg yr}^{-1}$ , which is divided up into the three sectors as indicated by the numbers at the upper-left corner.

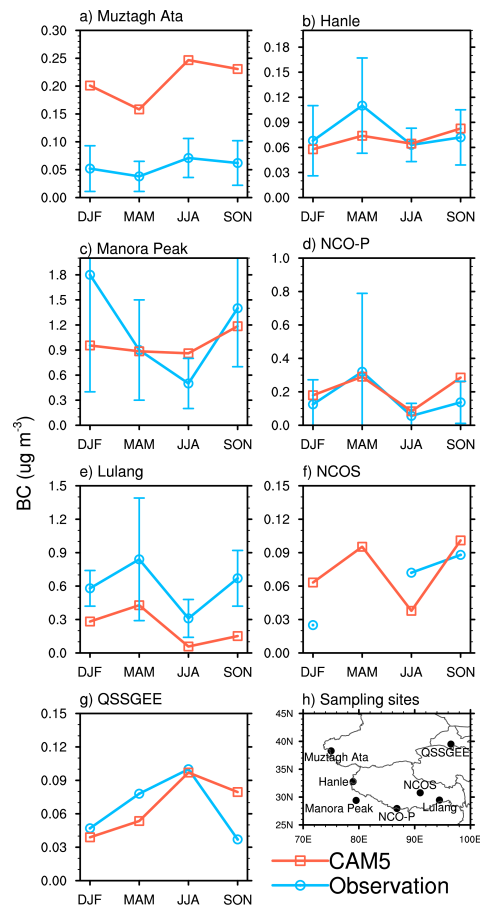


**Fig. 2.** Seasonal mean surface BC concentration ( $\mu\text{g m}^{-3}$ ) from observations (blue lines with error bars denoting SD) and CAM5 simulation (red lines) at the seven sampling sites listed in Table 1 and marked in map of panel h.



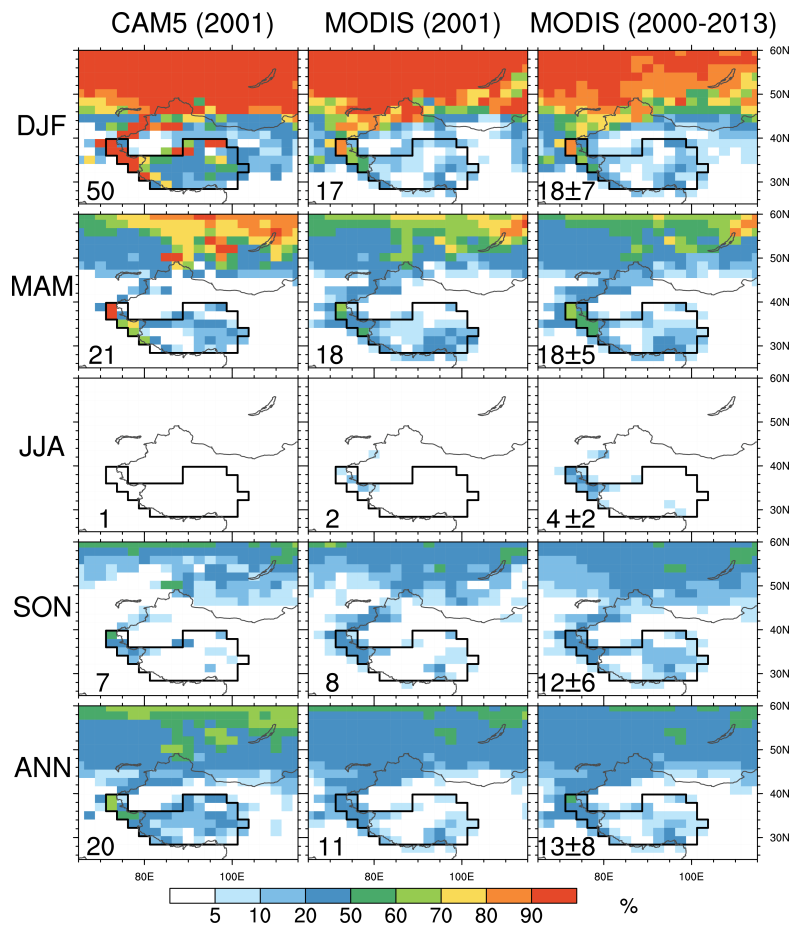


**Fig. 3.** Seasonal and annual mean snow cover fraction from CAM5 simulation for year 2001 (left), and MODIS retrieval for 2001 (middle) and 2000-2013 (right). The summer (JJA) in 2001 for both CAM5 and MODIS only includes July and August due to missing MODIS data in June. The number in the lower-left corner of each panel is the corresponding spatial mean SCF for the HTP region (which is marked with black outline), and for MODIS the standard deviation calculated from the MODIS multi-year means is also included.

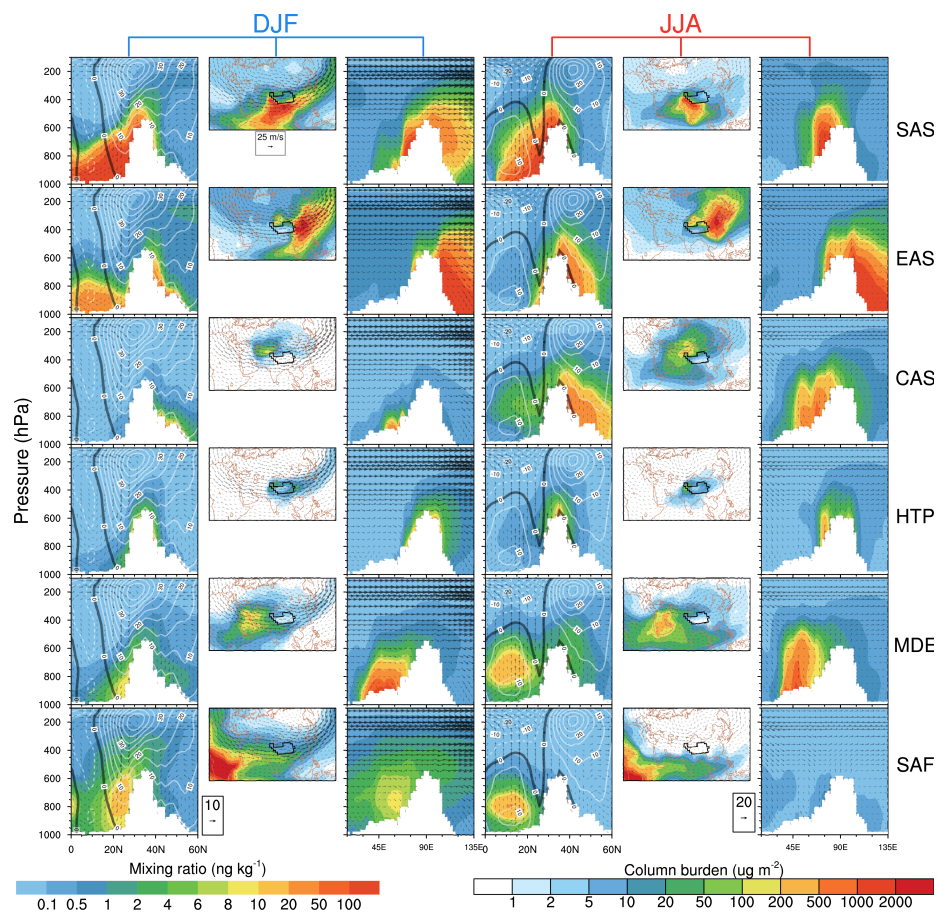


**Fig. 4.** The first column shows the latitude-height distributions of DJF BC mass mixing ratios (in  $\text{ng kg}^{-1}$ , colors) averaged over  $71.25\text{--}101.25^\circ\text{E}$ , originating from BB and FF sectors in the tagged source regions (corresponding to different rows); the white shaded area denotes topography, and the superimposed white contours at intervals of  $5 \text{ m s}^{-1}$  represent the westerly (solid) and easterly (dashed) DJF mean zonal winds along the cross-section with the thick solid black contour at  $0 \text{ m s}^{-1}$ ; the wind vectors (consisting of vertical velocity in units of  $10^{-4} \text{ hPa s}^{-1}$  and meridional wind in  $\text{m s}^{-1}$ ) are represented by arrows. Colors in the second column denote spatial distribution of the DJF mean BC column burden (in  $\mu\text{g m}^{-2}$ ), originating from different source regions, and the arrows represent the DJF mean horizontal wind vectors at 500hPa; the HTP is marked with black outline. The third column is similar to the first column except that the quantities are on the longitude-height cross-section averaged over  $28\text{--}40^\circ\text{N}$ , and thus the horizontal component of the wind vectors is zonal wind ( $\text{m s}^{-1}$ ) instead. The fourth to sixth columns are the same as the first to third columns, respectively, but for JJA means instead.

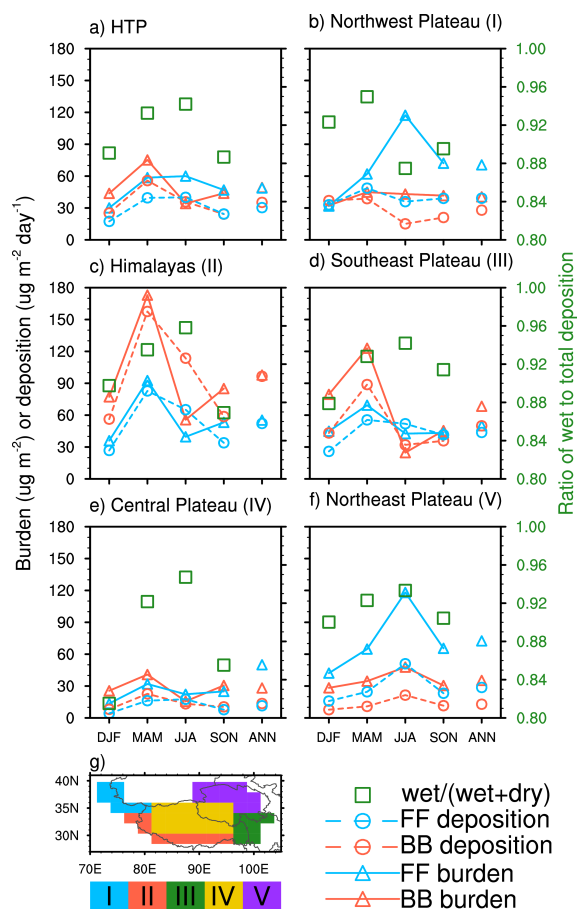


**Fig. 5.** Seasonal and annual mean BC column burden (solid lines and open triangles, in  $\mu\text{g m}^{-2}$ ) and deposition rate (dashed lines and open circles, in  $\mu\text{g m}^{-2} \text{ day}^{-1}$ ) over (a) the HTP, (b) Northwest Plateau, (c) Himalayas, (d) Southeast Plateau, (e) Central Plateau and (f) Northeast Plateau, emitted from BB (red color) and FF (blue color) source sectors. The green squares denote the ratio of wet to total BC deposition (using y-axis on the right) in four seasons over each receptor region. The geographical locations of five sub-regions of HTP are indicated in panel g.

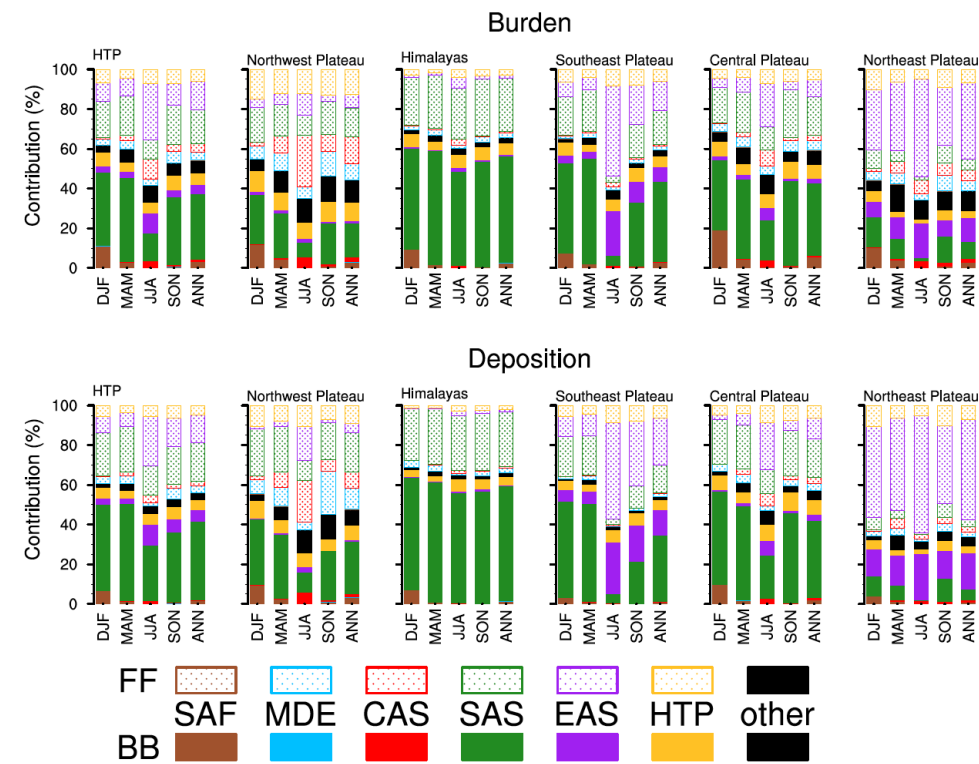
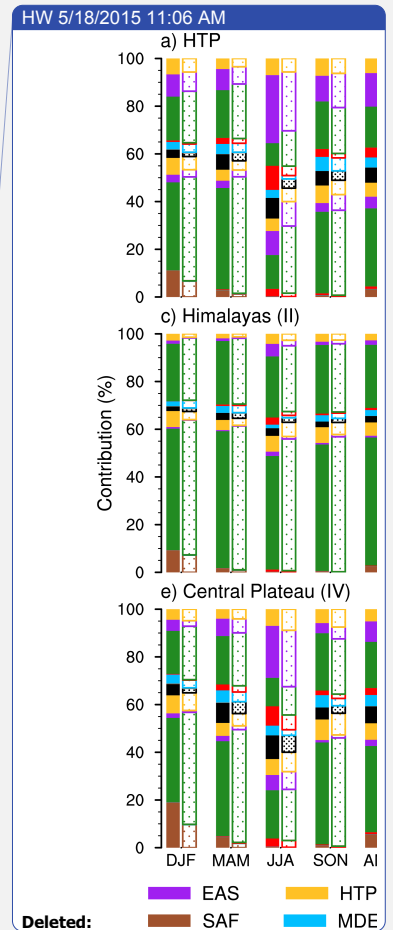


**Fig. 6.** Fractional contributions (measured by the lengths of color bars) to seasonal and annual mean BC column burden (top 6 panels) and deposition (bottom 6 panels) over the HTP, Northwest Plateau, Himalayas, Southeast Plateau, Central Plateau, and Northeast Plateau, originating from six major tagged source regions (indicated by colors) for BB (solid bar) and FF (dotted bar) emissions. The black bar in each column represents the contribution from all of the other tagged source regions and sectors combined.



Deleted: HW 5/18/2015 11:06 AM Deleted: solid pattern bars...op 6 panels) at ... [1]

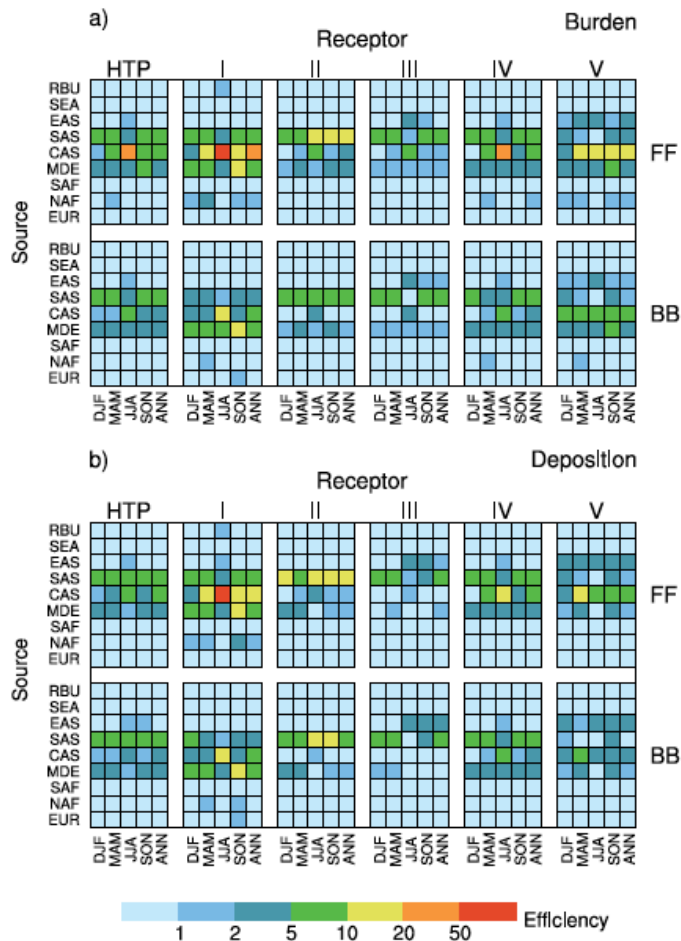


**Fig. 7.** Efficiency of FF (top) and BB (bottom) emissions from ten source regions (on the y-axis) in changing seasonal and annual mean (a) BC column burden and (b) deposition over the HTP and each of the five sub-regions: Northwest Plateau (I), Himalayas (II), Southeast Plateau (III), Central Plateau (IV) and Northeast Plateau (V).

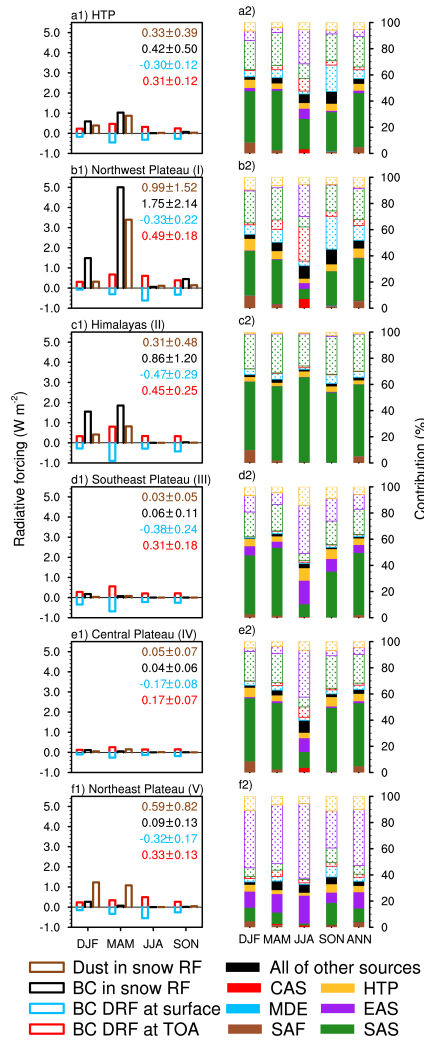


**Fig. 8.** Seasonal mean radiative forcing (left column) induced by the various BC effects (indicated by the color legend at the bottom) and dust-in-snow effect over (a1) the HTP, (b1) Northwest Plateau, (c1) Himalayas, (d1) Southeast Plateau, (e1) Central Plateau and (f1) Northeast Plateau. The corresponding annual mean forcings and one SD (for 12 monthly means) are shown in numbers on the top-right corner of each panel. The right column (a2-f2) panels represent source contribution to surface BC-in-snow radiative forcing over the corresponding receptors from tagged source regions (colors) and sectors (solid pattern bar and dotted pattern bar for BB and FF, respectively). The black bar in each column represents the contribution from all of the other tagged source regions and sectors.